

Vision-Language Models for Medical Report Generation and Visual Question Answering: A Review

Iryna Hartsock^{1,*}, Ghulam Rasool¹

¹Department of Machine Learning, H. Lee Moffitt Cancer Center & Research Institute, Tampa, FL, USA

Correspondence*:

Iryna Hartsock
iryna.hartsock@moffitt.org

2 ABSTRACT

3 Medical vision-language models (VLMs) combine computer vision (CV) and natural language
4 processing (NLP) to analyze visual and textual medical data. Our paper reviews recent
5 advancements in developing VLMs specialized for healthcare, focusing on publicly available
6 models designed for medical report generation and visual question answering (VQA). We provide
7 background on NLP and CV, explaining how techniques from both fields are integrated into VLMs,
8 with visual and language data often fused using Transformer-based architectures to enable effective
9 learning from multimodal data. Key areas we address include the exploration of 18 public medical
10 vision-language datasets, in-depth analyses of the architectures and pre-training strategies of
11 16 recent noteworthy medical VLMs, and comprehensive discussion on evaluation metrics for
12 assessing VLMs' performance in medical report generation and VQA. We also highlight current
13 challenges facing medical VLM development, including limited data availability, concerns with data
14 privacy, and lack of proper evaluation metrics, among others, while also proposing future directions to
15 address these obstacles. Overall, our review summarizes the recent progress in developing VLMs to
16 harness multimodal medical data for improved healthcare applications.

17 **Keywords:** vision-language models, report generation, visual question answering, datasets, evaluation metrics, healthcare

1 INTRODUCTION

18 The last decade has seen significant progress in artificial intelligence (AI) and machine learning (ML),
19 including the development of foundation models (FMs), large language models (LLMs), and vision-
20 language models (VLMs). These AI/ML developments have started transforming several aspects of our
21 daily lives, including healthcare. AI/ML can potentially transform the healthcare continuum by significantly
22 optimizing and improving disease screening, diagnostics, treatment planning, and post-treatment care
23 Bajwa et al. (2021). Various computer vision (CV) and natural language processing (NLP) models,
24 particularly LLMs, have been instrumental in driving this transformative trend He et al. (2023b); Zhou
25 et al. (2023b). CV models have been trained and validated for various screening and diagnosis use cases
26 leveraging radiology data from X-rays, mammograms, magnetic resonance imaging (MRI), computed
27 tomography (CT), and others. Recently, AI models focused on digital pathology using histopathology and
28 immunohistochemistry data have also shown significant advances in accurate disease diagnosis, prognosis,

29 and biomarker identification Waqas et al. (2023, 2024a). On the other hand, by training models using large
30 datasets of medical literature, clinical notes, and other healthcare-related text, LLMs can extract insights
31 from electronic health records (EHR) efficiently, assist healthcare professionals in generating concise
32 summary reports, and facilitate the interpretation of patient information. Noteworthy examples of such
33 LLMs include *GatorTron* Yang et al. (2022), *ChatDoctor* Li et al. (2023c), *Med-PaLM* (Medical Pathways
34 Language Model) Singhal et al. (2023) and *Med-Alpaca* Han et al. (2023).

35 The healthcare data is inherently multimodal, and consequently, the AI/ML models often need to be
36 trained using multiple data modalities, including text (e.g., clinical notes, radiology reports, surgical
37 pathology reports, etc.), imaging (e.g., radiology scans, digitized histopathology slides, etc.), and tabular
38 data (e.g., numerical data such as vitals or labs and categorical data such as race, gender, and others)
39 Acosta et al. (2022); Shrestha et al. (2023); Waqas et al. (2024b); Tripathi et al. (2024a); Mohsan et al.
40 (2023); Waqas et al. (2024c,a); Tripathi et al. (2024b). In routine clinical practice, healthcare professionals
41 utilize a combination of these data modalities for diagnosing and treating various conditions. Integrating
42 information from diverse data modalities enhances the precision and thoroughness of disease assessments,
43 diagnoses, treatment planning, and post-treatment surveillance. The need for AI/ML models to ingest,
44 integrate, and learn from information stemming from varied data sources is the driving force for *multimodal*
45 *learning* Huang et al. (2021); Waqas et al. (2024b).

46 The recent progress in multimodal learning has been driven by the development of VLMs Gan et al.
47 (2022); Chen et al. (2023); Mohsan et al. (2023). These models analyze, interpret, and derive insights from
48 both visual and textual data. In the medical domain, these models contribute to a holistic understanding of
49 patient information and improve ML model performance in clinical tasks. Many of these models, like *CLIP*
50 (Contrastive Language–Image Pre-training) Radford et al. (2021), *LLaVa* (Large Language and Vision
51 Assistant) Liu et al. (2023c), and *Flamingo* Alayrac et al. (2022) are tailored to healthcare domain through
52 training on extensive medical datasets. Adapting VLMs for medical visual question-answering (VQA)
53 Lin et al. (2023b) enables healthcare professionals to query medical images such as CT scans, MRIs,
54 mammograms, ultrasounds, X-rays, and more. The question-answering capability elevates the interactive
55 nature of the AI/ML models in healthcare, facilitating dynamic exchanges between healthcare providers
56 and the AI system. Furthermore, adapting VLMs for medical report generation enables them to amalgamate
57 information from visual and textual sources, producing detailed and contextually relevant reports. This
58 enhances healthcare workflow efficiency by ensuring comprehensive and accurate reports.

59 In contrast to previous related surveys Lin et al. (2023b); Ting et al. (2023); Shrestha et al. (2023), this
60 review aims to provide a comprehensive update on how methods from CV and NLP are integrated to
61 develop VLMs specifically designed for medical report generation and VQA. The specific objectives of
62 this review are as follows:

- 63 • Provide essential background on artificial neural networks, CV, and NLP, to ensure the accessibility
64 of this review for readers from medical fields and promote collaboration and knowledge exchange
65 between the AI/ML community and the medical professionals (see Section 2).
- 66 • Explore the integration of CV and NLP in VLMs, including model architectures, training strategies,
67 and downstream tasks (see Section 3).
- 68 • Analyze recent advances in VLMs, datasets, and evaluation metrics relevant to medical report
69 generation and VQA (see Section 4). Specifically:
 - 70 • Describe 18 publicly available vision-language datasets that encompass medical image-text pairs or
71 question-answer pairs related to medical images (see Section 4.1).

- Outline over 10 metrics employed for evaluating VLMs in the context of report generation and VQA tasks (see Section 4.2).
- Thoroughly review 16 recent medical VLMs, 15 of which are publicly available, with most models not previously covered in other surveys (see Section 4.3).
- Discuss the current challenges within the field of medical VLMs, offering insights into potential research directions that could profoundly influence their future development (see Section 5).

The overall structure of this review is shown in Figure 1. The list of medical VLMs and datasets can also be found on GitHub.

2 MACHINE LEARNING (ML) - A BRIEF REVIEW

Deep learning (DL), a subfield of ML, involves algorithms that learn to recognize patterns and make decisions by analyzing large amounts of data. In this section, we review the fundamental principles of DL and explore two main areas of DL relevant to medical VLMs: CV and NLP. For more detailed information on DL, we refer the reader to LeCun et al. (2015); Goodfellow et al. (2016); Baldi (2021).

2.1 Principles of Deep Learning (DL)

ML and AI originated in the 1940s-1950s, with neural networks (NNs) emerging as classical models. The fundamental building block of an NN is an artificial neuron, which receives multiple inputs, aggregates them, applies nonlinear operations, and outputs a single scalar value. NNs consist of layers of interconnected artificial neurons, including input, output, and hidden layers. In feedforward NNs, connections are structured so that a connection from neuron i to neuron j exists only if $i < j$ Baldi (2021). In any NN, the connections between artificial neurons carry weight, and neurons utilize “activation functions” on their inputs to introduce non-linearity. An activation function is a mathematical operation that transforms the weighted sum of inputs into an output, enabling the network to model complex patterns. Common activation functions include the sigmoid, hyperbolic tangent (tanh), and Rectified Linear Unit (ReLU).

A loss function quantifies the disparity between predicted and actual outputs, with the goal of minimizing this scalar value during training. DL leverages NNs but extends them into deeper architectures with many hidden layers. Backpropagation, short for backward propagation of errors, is essential for training deep NNs. It involves calculating the gradient of the loss function with respect to the weights, using the chain rule for derivatives Baldi (2021). This gradient information updates the weights to minimize the loss. Common optimization methods include gradient descent, stochastic gradient descent (SGD) Robbins (1951), and Adam (Adaptive Moment Estimation) Kingma and Ba (2014). These methods iteratively update the weights to improve the model’s performance during training.

2.2 Natural Language Processing (NLP)

NLP is the analysis of linguistic data, most commonly in the form of textual data such as documents or publications, using computational methods Verspoor and Cohen (2013). NLP encompasses a variety of tasks aimed at understanding, processing, and generating human language. The common NLP tasks include machine translation, named entity recognition, text summarization, etc. In the following, we introduce terminology and fundamental concepts that will help the reader in the coming sections on modern NLP and medical VLMs.

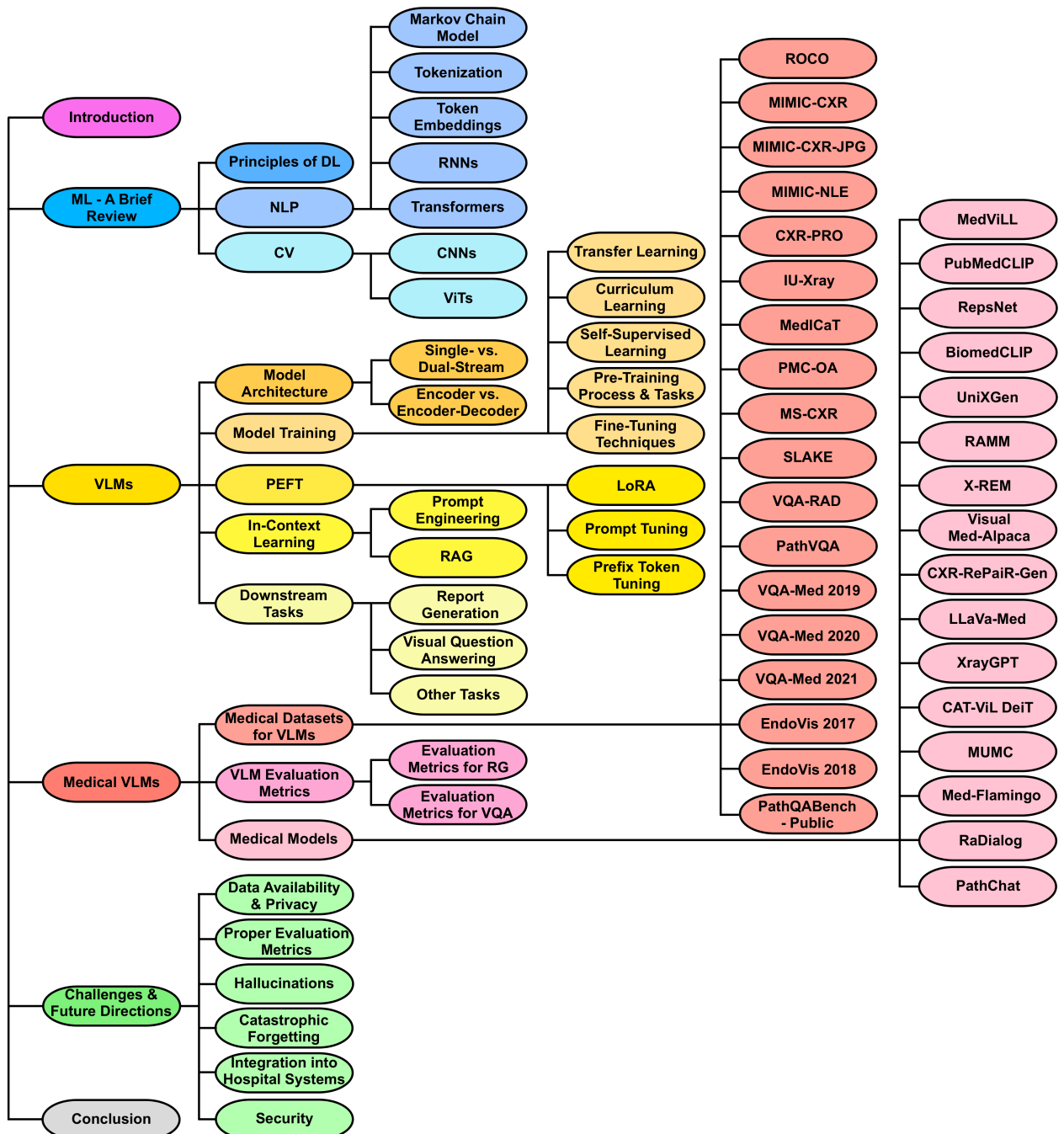


Figure 1. Organization of the review paper. The structure begins with an introduction, followed by a foundational review of ML and background on VLMs. It then delves into medical vision-language datasets, evaluation metrics, and recent medical VLMs. Next, the paper addresses the current challenges of medical VLMs and proposes possible future research directions. It ends with a conclusion summarizing key insights and findings.

109 2.2.1 Markov Chain Model

110 The Markov chain model has historically been significant in NLP, particularly for tasks involving sequence
 111 prediction and probabilistic modeling of text data Nadkarni et al. (2011). A Markov chain is a stochastic
 112 process that transitions from one state to another based on specific probabilistic rules, with the fundamental

113 property that the future state depends only on the current state and not on the sequence of events that
114 preceded it. This property, known as the Markov property, allowed Markov chains to model the likelihood
115 of sequences of words or characters by capturing statistical dependencies between adjacent elements.
116 They facilitated tasks such as text generation, next-element prediction, and part-of-speech tagging in early
117 NLP research and applications, providing a foundational framework for subsequent advanced techniques
118 Nadkarni et al. (2011).

119 2.2.2 Tokenization

120 In contemporary NLP, tokenization is the initial step involving the splitting of sentences and words into
121 their smallest morphemes, known as tokens Rai and Borah (2021). Subword tokenization methods are
122 often preferred in many NLP applications due to their effectiveness in handling out-of-vocabulary words.
123 *WordPiece* Wu et al. (2016) starts by treating each character as a token, forming an initial vocabulary. Using
124 a flexible merging strategy, WordPiece considers adjacent characters or subword units that enhance the
125 overall likelihood of the training data, aiming to accurately represent it given the model's current state.
126 *Byte-Pair Encoding (BPE)* Sennrich et al. (2016) shares similarities with WordPiece but follows a more
127 deterministic merging strategy. BPE merges the most frequent pair of adjacent characters or subword units
128 in each iteration, progressing toward a predefined vocabulary size. *Byte-level BPE* Wang et al. (2020)
129 operates at an even finer granularity, considering individual bytes instead of characters. This extension
130 allows it to capture more nuanced patterns at the byte level.

131 2.2.3 Token Embeddings

132 Tokens are often transformed into numerical vectors that capture semantic relationships between tokens,
133 called word or token embeddings. *Word2Vec* Mikolov et al. (2013b) is a widely used word embedding
134 technique employing two models: Skip-Gram Mikolov et al. (2013b) and Continuous Bag of Words
135 (CBOW) Mikolov et al. (2013a). Skip-Gram predicts context words given a target word, capturing
136 semantic associations, while CBOW predicts the target word based on context, emphasizing syntactic
137 structures. Word2Vec is computationally efficient, making it suitable for large datasets and general-purpose
138 applications. *Global Vectors (GloVe)* Pennington et al. (2014) focuses on capturing global semantic
139 relationships by analyzing word pair statistics across the entire corpus. It generates word vectors reflecting
140 co-occurrence probabilities, which is ideal for tasks requiring a holistic understanding of word connections.
141 *FastText* Bojanowski et al. (2017) is effective for handling out-of-vocabulary words and morphologically
142 rich languages. It adopts a sub-word approach, breaking words into n-grams, and uses a skip-gram training
143 method similar to Word2Vec to learn embeddings for these sub-word units.

144 Specialized embeddings are available for biomedical and clinical terms. *BioWordVec* Zhang et al. (2019)
145 incorporates MeSH terms and text from PubMed abstracts to learn improved biomedical word embeddings.
146 *Cui2vec* Beam et al. (2020) utilizes multi-modal data from medical publications and clinical notes, mapping
147 terms onto a common Concept Unique Identifier (CUI) space. Additionally, *positional encodings*, often
148 based on sinusoidal functions, are commonly added to capture the order of tokens in a sequence. These
149 vectors systematically encode token positions, enriching embeddings with positional information for
150 tailored NLP tasks Ahmed et al. (2023).

151 2.2.4 Recurrent Neural Networks (RNNs)

152 RNNs are widely employed for pattern detection in sequential data like genomic sequences, text, or
153 numerical time series Schmidt (2019). Operating on the principle of preserving a form of memory, RNNs
154 incorporate a cyclic structure by looping the output of a specific layer back to the input, facilitating the

155 prediction of subsequent layer outputs. This mechanism empowers RNNs to adeptly model sequential and
156 temporal dependencies, capturing information from preceding time steps within hidden states. However,
157 they face challenges in retaining long-term dependencies due to the vanishing gradient problem. To address
158 this, variants like Long Short-Term Memory (LSTM) Hochreiter and Schmidhuber (1997) and Gated
159 Recurrent Unit (GRU) Cho et al. (2014) have been developed to better capture and utilize long-range
160 dependencies in sequential data Ahmed et al. (2023).

161 2.2.5 Transformers

162 In recent years, there has been a remarkable advancement in NLP mainly due to the development of the
163 Transformer models Vaswani et al. (2017). Beyond incorporating embeddings and positional encodings, the
164 Transformer architecture consists of an encoder that processes input data, represented by vectors obtained
165 from embedded and positionally encoded tokens. The encoder-generated representation then serves as
166 the input for the subsequent decoder, transforming these vector representations into a relevant output
167 tailored to the specific task. A defining characteristic of the Transformer lies in its *self-attention* mechanism,
168 particularly the scaled dot-product attention, which proves instrumental in capturing intricate dependencies
169 within sequences.

170 The synergy between enhanced computational power provided by Graphical Processing Units (GPUs)
171 and advancements in attention mechanisms has been pivotal in developing large language models (LLMs).
172 These models are meticulously trained on vast datasets with many parameters. BERT (Bidirectional
173 Encoder Representations from Transformers) Devlin et al. (2019) marked the inception of LLMs. The era
174 of even larger LLMs began in 2020 with the introduction of models like GPT-3 (the 3rd generation of the
175 Generative Pre-trained Transformer model) Brown et al. (2020) and PaLM (Pathways Language Model)
176 Chowdhery et al. (2022). Some recent LLMs include LLaMA (Large Language Model Meta AI Touvron
177 et al. (2023a,b), Vicuna Chiang et al. (2023), and Mistral Jiang et al. (2023).

178 2.3 Computer Vision (CV)

179 CV involves interpreting and understanding the world from their images or videos Ji (2020). Data in
180 CV is encoded as numerical values representing the intensity or brightness of pixels. The extraction of
181 visual patterns like edges, textures, and objects in images or video frames serves as building blocks for
182 various CV tasks like image classification, object detection, and semantic segmentation. **In the following,**
183 **we introduce fundamental concepts and terms essential for understanding VLMs presented in the later**
184 **parts of the paper.**

185 2.3.1 Convolutional Neural Networks (CNNs)

186 CNNs represent a significant advancement in CV Yamashita et al. (2018). Besides pooling and fully
187 connected layers, CNNs also have convolution layers, which apply convolution operations to input data. A
188 small filter or kernel slides over the input data during a convolution operation, performing element-wise
189 multiplications with local regions of the input at each position. The results are summed to create a new
190 value in the output feature map. This process is repeated across the entire input, capturing patterns and
191 features at different spatial locations. The well-known CNNs include Residual Network (ResNet) He et al.
192 (2016), Dense Convolutional Network (DenseNet) Huang et al. (2022), Efficient Network (EfficientNet)
193 Tan and Le (2020) and others.

194 2.3.2 Vision Transformers (ViTs)

195 Transformer models, originally proposed for NLP tasks, have also found valuable applications in CV.
196 For instance, the ViT model Dosovitskiy et al. (2021) can capture intricate relationships and dependencies
197 across the entire image. This is achieved by leveraging the Transformer architecture and treating images as
198 sequences of smaller patches. Each image patch undergoes flattening into a vector, followed by passage
199 through an embedding layer, enriching the patches for a more expressive representation. Positional
200 encodings are then incorporated to convey spatial arrangement information. ViTs also introduce a
201 special token capturing global image information, represented by a learnable token embedding with
202 unique parameters. ViTs have excelled in semantic segmentation Ranftl et al. (2021), anomaly detection
203 Mishra et al. (2021), medical image classification Manzari et al. (2023); Barhoumi et al. (2023) and even
204 outperformed CNNs in some cases Tyagi et al. (2021); Xin et al. (2022).

3 VISION-LANGUAGE MODELS (VLMs)

205 Many real-world scenarios inherently involve multiple data modalities, prompting the development of
206 VLMs capable of simultaneously handling and understanding both NLP and CV data. **In this section, we**
207 **build on the basic concepts described earlier and present VLMs, their architectures, training and fine-tuning**
208 **methods, and various downstream tasks facilitated by these multimodal models.**

209 3.1 Model Architecture

210 3.1.1 Single-**Stream** vs. Dual-Stream VLMs

211 Based on how different data modalities are fused together in VLMs, they are generally categorized
212 into two groups Chen et al. (2023): (1) *single-stream* (e.g., VisualBERT Li et al. (2019) and UNITER or
213 UNiversal Image-TExt Representation Learning Chen et al. (2020b)), and (2) *dual-stream* models (e.g.,
214 ViLBERT or Vision-and-Language BERT Lu et al. (2019) and CLIP or Contrastive Language-Image
215 Pre-training Radford et al. (2021)).

216 A **single-stream** VLM adopts an efficient architecture for processing visual and textual information
217 within a unified module (see Figure 2 A and **and Figure 3 A**). This architecture incorporates an early fusion
218 of distinct data modalities, concatenating feature vectors from various data sources into a single vector (e.g.,
219 MedViLL Moon et al. (2022)). Subsequently, this combined representation is fed into a single stream. One
220 notable advantage of the single-stream design is its parameter efficiency, achieved by employing the same
221 set of parameters for all modalities. This simplifies the model and contributes to computational efficiency
222 during training and inference phases Chen et al. (2023).

223 A **dual-stream** VLM extracts visual and textual representations separately in parallel streams without
224 parameter sharing (see Figure 2 B **and Figure 3 B**). This architecture typically exhibits higher computational
225 complexity than single-stream architectures. Visual features are generated from pre-trained *vision encoders*,
226 such as CNNs or ViTs, and textual features are obtained from pre-trained *text encoders*, usually based on the
227 Transformer architecture (e.g., PubMedCLIP Eslami et al. (2023)). These features are then integrated using
228 a *multimodal fusion module*, often leveraging attention mechanisms, to capture cross-modal dependencies.

229 3.1.2 Encoder vs. Encoder-Decoder VLMs

230 The learned cross-modal representations can be optionally processed by a *decoder* before producing
231 the final output. Consequently, VLMs are classified into two groups: (1) *encoder-only* (e.g., ALIGN (A

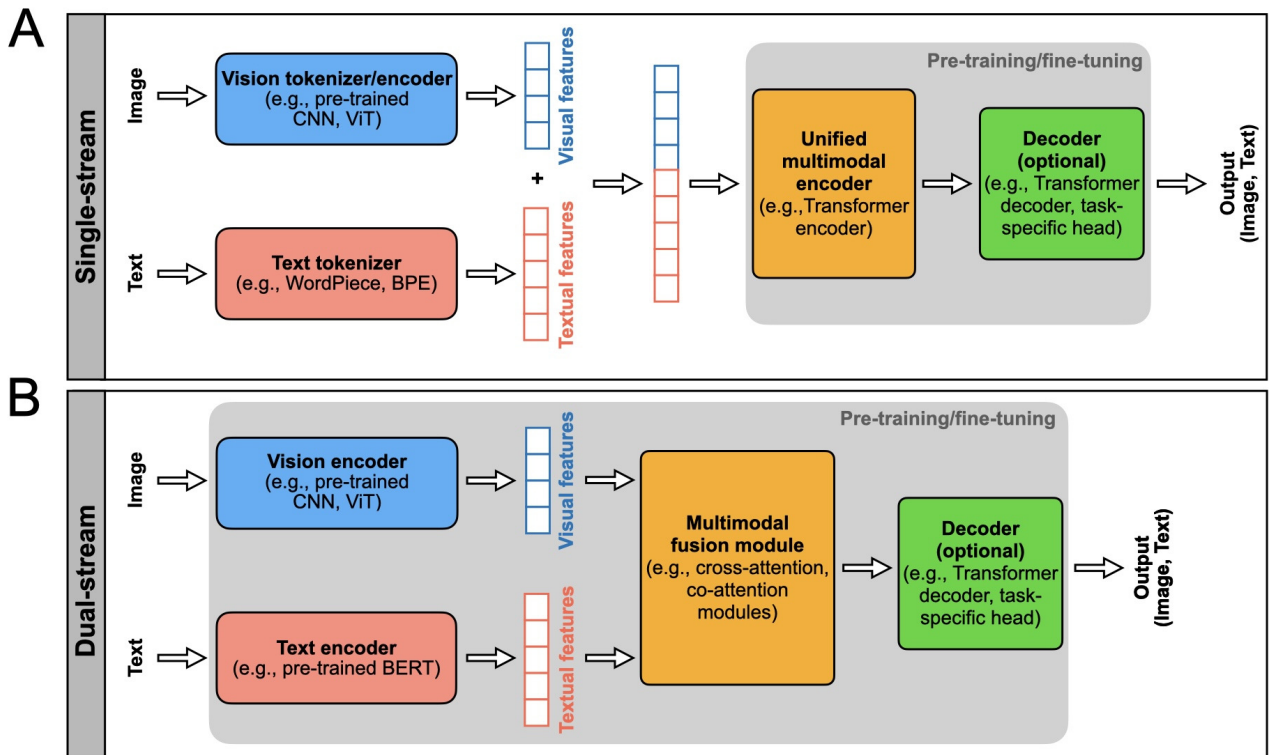


Figure 2. Two main types of VLM architectures, single-stream and dual-stream, are presented. The model inputs and outputs are indicated. The rectangular boxes inside the grey areas indicate the components of the VLM that **typically** undergo pre-training and fine-tuning, i.e., the model parameters are updated using labeled or unlabeled data. The top row (A) shows the single-stream VLM architecture, and the bottom row shows the (B) dual-stream. Each block indicated in these architectures can be designed using different AI/ML models as indicated in these blocks.

232 Large-scale Image and Noisy-text embedding) Jia et al. (2021)), and (2) *encoder-decoder* models (e.g.,
 233 SimVLM (Simple Visual Language Model) Wang et al. (2022c)).

234 **Encoder-only** VLMs are advantageous in scenarios where the primary objective is efficient representation
 235 learning. They often exhibit streamlined processing and reduced computational complexity, making them
 236 suitable for tasks requiring compact and informative representations. However, these models might lack
 237 the capability to generate intricate and detailed outputs, limiting their use in tasks demanding nuanced
 238 responses or creative generation.

239 **Encoder-decoder** VLMs offer the flexibility to generate complex and diverse outputs, making them
 240 well-suited for tasks like image captioning, translation, or any application requiring creative responses. The
 241 decoding step allows for the transformation of joint representations into meaningful outputs. However, this
 242 versatility comes at the cost of increased computational demand and complexity.

243 3.2 Model Training

244 3.2.1 Transfer Learning

245 A widely used strategy in ML is transfer learning, where pre-trained models are customized for specific
 246 downstream tasks. This involves fine-tuning the model's parameters using smaller task-specific datasets to
 247 address the intricacies of the target task rather than starting with random initialization Bommasani et al.
 248 (2022). Transfer learning often entails modifying the original model's architecture, such as adjusting final

A	Single-stream	B	Dual-stream
<p>Pros:</p> <ul style="list-style-type: none"> - Facilitates tight integration of visual and language features, as they are aligned early in the process; - Has simpler architecture, leading to easier implementation. <p>Cons:</p> <ul style="list-style-type: none"> - May struggle to capture the complexities and nuances of both vision and language data; - Often has difficulty adapting to diverse tasks. <p>Applications in Healthcare:</p> <ul style="list-style-type: none"> - Suited for straightforward medical VQA tasks where questions and images are tightly coupled; - Efficient for generating concise routine reports that summarize key visual findings from imaging (e.g., nodules, fluid); - Efficient for large-scale deployment in clinical settings with limited computational resources. 	<p>Pros:</p> <ul style="list-style-type: none"> - Extracts nuanced features from both vision and language data; - Adaptable across a wide range of tasks. <p>Cons:</p> <ul style="list-style-type: none"> - Features more complex architecture due to separate processing streams for visual and language data, requiring sophisticated design; - Typically demands more computational resources and memory. <p>Applications in Healthcare:</p> <ul style="list-style-type: none"> - Suited for complex medical VQA tasks that require fine-grained analysis of medical images; - Suited for intricate report generation in challenging clinical cases; - Adaptable to varying types of medical images (e.g., X-rays, MRIs, CT scans) through specialization of the visual stream. 		

Figure 3. Comparison of (A) single-stream and (B) dual-stream VLMs in terms of their advantages, disadvantages, and healthcare applications, to guide the selection of the appropriate architecture for various medical scenarios. In some cases, the optimal choice between architectures remains uncertain and may depend on specific task requirements.

249 layers or introducing new ones, like classification or regression layers, to align with the task requirements
 250 Bommasani et al. (2022). The goal is to adapt the pre-trained model to the new task while leveraging the
 251 knowledge it gained during initial pre-training. **Almost all VLMs use transfer learning during training in**
 252 **one way or another.**

253 3.2.2 Curriculum Learning

254 Curriculum learning offers a novel approach for tasks or data with inherent progressions or hierarchies. It
 255 strategically presents training examples or tasks in a designed order, often based on difficulty or complexity
 256 measures Soviany et al. (2021). For instance, LLaVa-Med, a recent medical VLM Li et al. (2023a), employs
 257 curriculum learning during training. This gradual learning approach starts with simpler examples and
 258 progresses to more complex ones, enhancing the model's adaptability and performance.

259 3.2.3 Self-Supervised Learning (SSL)

260 SSL provides a potent alternative to traditional supervised learning by enabling models to generate their
 261 own labels from data Rani et al. (2023). This approach is especially advantageous when acquiring labeled
 262 data is difficult or costly. In self-supervised learning for VLMs, models formulate tasks that leverage
 263 inherent data structures, allowing them to learn meaningful representations across modalities without

264 external labels. Examples of such tasks include contrastive learning, masked language modeling, and
265 masked image modeling (further detailed in the subsequent sub-section).

266 3.2.4 Pre-Training Process and Tasks

267 The pre-training process is crucial for providing VLMs with a foundational understanding of the complex
268 relationship between visual and textual data. A common approach involves extensive pre-training on
269 datasets pairing images/videos with their corresponding textual descriptions. Throughout pre-training,
270 the model engages in various tasks to acquire versatile representations for downstream applications. **The
271 following paragraphs describe commonly used pre-training techniques.**

272 **Contrastive Learning (CL)** trains the model to distinguish positive pairs from negative pairs of visual
273 and textual data Li et al. (2021). Positive pairs contain related visual and textual content, like an image
274 with its corresponding description. Negative pairs contain unrelated content, such as an image paired with
275 a randomly chosen description. The goal is to bring positive pairs closer and push negative pairs apart in a
276 shared embedding space. Various contrastive loss functions are used, with InfoNCE (Noise-Contrastive
277 Estimation) loss van den Oord et al. (2019) being a common choice. CLIP Radford et al. (2021) employs
278 InfoNCE with cosine similarity, while ALIGN Jia et al. (2021) uses normalized softmax loss to enhance
279 positive similarity and reduce negative similarities.

280 **Masked Language Modeling (MLM)** is an NLP task Taylor (1953) first utilized in BERT Devlin et al.
281 (2019). MLM randomly replaces a percentage of tokens in textual data with a special token, usually denoted
282 as MASK. The model then predicts these masked tokens, considering the context on both sides, enabling it
283 to capture detailed contextual information. VLMs like UNITER Chen et al. (2020b) and VisualBERT Li
284 et al. (2019) utilize MLM during pre-training.

285 **Masked Image Modeling (MIM)**, extending the idea of MLM to images, emerged as a novel approach
286 Xie et al. (2022). In MIM, certain patches are masked, prompting the model to predict the contents
287 of masked regions. This process enables the model to draw context from the entirety of the image,
288 encouraging the integration of both local and global visual features. VLMs like UNITER Chen et al.
289 (2020b) and ViLBERT Lu et al. (2019) leverage MIM for enhanced performance. The *cross-entropy loss*
290 is employed in MLM and MIM tasks to measure the difference between predicted and actual probability
291 distributions for the masked elements. Additionally, MLM can be combined with MIM, allowing the
292 reconstruction of the masked signal in one modality with support from another modality Kwon et al. (2023).

293 **Image-Text Matching (ITM)** is another common vision-language pre-training task. Throughout the
294 training, the model learns to map images and corresponding textual descriptions into a shared semantic
295 space, where closely aligned vectors represent similar content in both modalities. In single-stream VLMs,
296 the special token [CLS] represents the joint representation for both modalities. In contrast, in dual-
297 stream VLMs, the visual and textual representations of $[CLS]_V$ and $[CLS]_T$ are concatenated. This joint
298 representation is fed into a fully-connected layer followed by the sigmoid function, predicting a score
299 indicating match or mismatch Chen et al. (2023). Models like CLIP Radford et al. (2021) and ALBEF
300 (ALign the image and text representations BEfore Fusing) Li et al. (2021) leverage ITM during pre-training.

301 In VLM pre-training, multiple tasks are often combined to enable models to understand nuanced
302 contextual information across modalities. Tasks like contrastive loss, cross-entropy loss for masked token
303 prediction, and others can be integrated into the final loss function. This approach equips VLMs with
304 versatile representations for diverse downstream tasks. For instance, ALBEF Li et al. (2021) adopts a

305 pre-training objective involving CL, MLM, and ITM tasks, with the overall loss computed as the sum of
306 these components.

307 3.2.5 Fine-Tuning Techniques

308 Following the training, a common practice involves fine-tuning VLMs on smaller datasets tailored to
309 specific downstream tasks. **In the following, we present well-known techniques for fine-tuning VLMs.**

310 **Supervised Fine-Tuning (SFT)** involves meticulous fine-tuning of a model on a dataset curated to match
311 the nuances of the targeted application. However, before engaging in SFT, the VLM undergoes pre-training
312 on an extensive image-text dataset to establish a foundational understanding of visual-textual relationships.
313 This dual-phase strategy enables the model to generalize broadly while adapting to specific applications
314 Ouyang et al. (2022).

315 **Reinforcement Learning from Human Feedback (RLHF)** is a distinct fine-tuning approach employed
316 to enhance VLMs through the incorporation of human preferences during fine-tuning Ouyang et al.
317 (2022); Lambert et al. (2022); Ziegler et al. (2020). RLHF initiates with an initial model, incorporating
318 human-generated rankings of its outputs to construct a detailed reward model. In contrast to traditional
319 reinforcement learning (RL) Sutton and Barto (1998); Coronato et al. (2020), which relies solely on
320 environmental interactions, RLHF strategically integrates human feedback. This human-in-the-loop
321 approach provides a more nuanced and expert-informed methodology, allowing for fine-tuning in alignment
322 with human preferences, ultimately improving model outcomes.

323 **Instruction Fine-Tuning (IFT)** refers to refining a pre-trained language model by providing specific
324 instructions or guidance tailored to a particular task or application Ren et al. (2024). This process typically
325 involves exposing the model to examples or prompts related to the desired instructions and updating
326 its parameters based on the feedback received during this task-specific training phase. Medical VLM,
327 RaDialog Pellegrini et al. (2023), employs this fine-tuning technique.

328 3.3 Parameter-Efficient Fine-Tuning (PEFT)

329 This section explores strategies for adapting VLMs while keeping the model's parameters frozen and only
330 updating newly added layers. PEFT has emerged as a prominent approach, focusing on optimizing parameter
331 utilization, especially in scenarios with limited labeled data for the target task. PEFT integrates task-specific
332 parameters, called *adapters*, into a pre-trained model while retaining its original parameters. Adapter
333 modules typically feature a bottleneck structure, projecting original features into a reduced dimension,
334 applying non-linearity, and then projecting back to the original dimension. This design ensures parameter
335 efficiency by minimizing the number of added parameters per task. Adapter modules, placed after each
336 layer of the pre-trained model, capture task-specific details while preserving shared parameters, enabling
337 seamless extension to new tasks without significant interference with previously acquired knowledge.

338 3.3.1 Low-Rank Adaptation (LoRA)

339 LoRA is a common adapter-based method Hu et al. (2022). The adaptation process involves fine-tuning
340 two smaller low-rank matrices that are decompositions of the larger weight matrix of the pre-trained
341 model. These smaller matrices constitute the LoRA adapter modules, and the approach focuses on making
342 low-rank modifications to adapt the model for specific tasks efficiently. Pre-trained LLMs that are part of
343 medical VLMs architecture are often fine-tuned using LoRA (e.g., Visual Med-Alpaca Shu et al. (2023)
344 and RaDialog Pellegrini et al. (2023)).

345 3.3.2 Prompt Tuning

346 Prompt tuning involves creating continuous vector representations as input hints Lester et al. (2021),
347 enabling the model to dynamically create effective prompts during training. This iterative process
348 significantly enhances the model's ability to generate contextually relevant responses and adapt its behavior
349 based on an evolving task. VLMs like Qwen-VL and InstructBLIP used prompt tuning Bai et al. (2023a);
350 Dai et al. (2023).

351 3.3.3 Prefix Token Tuning

352 Prefix token tuning adds task-specific vectors to the input, specifically to the initial tokens known as
353 *prefix tokens*, to guide the model's behavior for a given task Li and Liang (2021). For instance, VL-T5
354 utilized different prefixes for questions from various datasets Cho et al. (2021) . These vectors can be
355 trained and updated independently while the remaining pre-trained model parameters are frozen. Prefix
356 token tuning allows task-specific adaptation without compromising the pre-trained knowledge encoded in
357 most model parameters.

358 3.4 In-Context Learning

359 In this section, we explore strategies for adapting VLMs using the context only, keeping the model's
360 parameters (and PEFT/LoRA adapters, if any) frozen. In our settings, in-context learning may be considered
361 using LLMs or VLMs for inference only.

362 3.4.1 Prompt Engineering

363 Prompt engineering involves guiding a trained model with task-specific instructions, known as *prompts*,
364 to tailor its output for specific tasks Gu et al. (2023). Examples include instructing the model to generate a
365 radiology report for a specific image (e.g., RAMM Pellegrini et al. (2023)). Prompt engineering can also
366 expose the VLM to interconnected examples or prompts, guiding it to a desired output. Another approach
367 incorporates progressively structured instructions or questions, refining focus and enhancing the model's
368 ability to generate coherent and contextually relevant responses Gu et al. (2023).

369 3.4.2 Retrieval Augmented Generation (RAG)

370 RAG is a form of prompt engineering that involves strategically crafting prompts for both retrieval and
371 generation phases, allowing for an adaptive and efficient process that leverages external knowledge sources
372 to enhance generative tasks. While the original concept of RAG was developed in the context of NLP Lewis
373 et al. (2020), the principles behind retrieval and generation can be extended to multimodal learning Zhao
374 et al. (2023), including VLMs. RAG has been used in medical VLMs for tasks like VQA (e.g., RAMM
375 Yuan et al. (2023)) and RG (e.g., CXR-RePaiR-Gen Ranjit et al. (2023)). RAG begins with a retrieval
376 component, usually a pre-trained model designed for information retrieval. This versatile component
377 excels in extracting pertinent information from extensive datasets, catering to various modalities such as
378 images, text, codes, video, or audio when presented with diverse inputs Zhao et al. (2023). Following the
379 retrieval phase, the model returns a set of contexts related to the given input. The second component is a
380 generative LLM. This component takes the input and the retrieved context and generates the final output.
381 The generated output is conditioned on the input and the information extracted from the retrieved context.
382 An intrinsic advantage of RAG lies in its capacity to reduce the reliance on extensive labeled datasets.
383 While the base model is typically frozen during RAG, there are instances, as seen in RAMM Yuan et al.
384 (2023), where model parameters are updated in the process.

385 **3.5 Downstream Tasks**386 Multimodal downstream tasks leverage the acquired knowledge from pre-training VLMs to excel in
387 diverse applications that require a joint understanding of visual and textual data.388 **3.5.1 Report Generation (RG)**389 RG is a prominent example of a typical medical VLM task, which centers on creating a comprehensive
390 summary report of visual data. RG plays a crucial role in automatically summarizing diagnostic imaging
391 results and reducing the workload of report writing Monshi et al. (2020); Ting et al. (2023); Mohsan et al.
392 (2023). For instance, in radiology, a report generation system could analyze a set of medical images such
393 as X-rays, CT scans, or MRIs and generate a detailed report summarizing the observed abnormalities,
394 their locations, and potential implications for diagnosis or treatment Liu et al. (2023b). A radiology report
395 usually has several sections: (1) *Examination* (type of exam), (2) *Indication* (reasons for the examination),
396 (3) *Comparison* (prior exams), (4) *Technique* (scanning method) (5) *Findings* (detailed observations made
397 by a radiologist), and (6) *Impression* (summary of the major findings) Mabotuwana et al. (2020). In the
398 context of RG, VLMs are usually designed to generate *Findings* and *Impression* sections Thawkar et al.
399 (2023).400 Traditional methods of RG in radiology, such as handwriting, telephone dictation, transcriptionist-oriented
401 systems, speech recognition, and structured data entry, face several challenges, including medical errors,
402 cognitive overload, and inefficient decision-making. Handwriting and telephone dictation are particularly
403 vulnerable to mistakes, as they can suffer from issues like illegible handwriting and miscommunication,
404 leading to misinterpretations. Structured data entry, although designed to standardize and streamline
405 reporting, often places a significant cognitive burden on radiologists, who must meticulously input detailed
406 information, potentially leading to fatigue and errors. While technological advancements like electronic
407 health records (EHRs), improved speech recognition software, standardized reporting templates, and
408 automated error detection have been developed to mitigate these challenges, they have limitations. For
409 example, EHRs and speech recognition still require substantial manual input and proofreading, which can
410 be time-consuming and prone to error. Standardized reporting templates are helpful in ensuring consistency,
411 but they can be inflexible and may not always capture the nuanced details of individual cases. Automated
412 error detection systems are also not foolproof, often requiring human oversight to verify and correct flagged
413 issues. Despite these improvements, the need for manual effort and the potential for human error remain
414 significant concerns.415 The evolution of RG methods parallels the advancements in image captioning. Early methods in image
416 captioning included retrieval-based approaches, where captions were generated by retrieving existing
417 phrases from a database, and template-based approaches, where predefined sentence templates were filled
418 with identified image elements, such as objects, actions, or locations Bai and An (2018). However, these
419 approaches struggled with generating captions for unseen images. This limitation motivated the emergence
420 of DL methods for RG. Initial DL approaches utilized CNNs to extract visual features from images, which
421 were then processed by RNNs to generate text descriptions Ting et al. (2023). While this CNN-RNN
422 approach improved the flexibility of captioning, it still faced challenges in capturing complex relationships
423 between images and text outputs, and it struggled with generating longer, more comprehensive reports,
424 often required in the medical field. These challenges gradually led to the adoption of VLMs in medical RG.425 VLMs represent a transformative leap in medical RG by addressing the shortcomings of previous methods.
426 By simultaneously integrating imaging and textual data, VLMs are able to generate more comprehensive and
427 coherent reports. They also significantly reduce cognitive load by automating the creation of comprehensive

428 reports, thereby liberating clinicians from the repetitive and time-consuming task of manual report writing.
429 Furthermore, VLMs provide consistent interpretations of imaging data, which helps minimize the risk
430 of errors associated with clinician fatigue or oversight. Their capability to process large volumes of data
431 efficiently streamlines the reporting process, enhancing the overall effectiveness of medical practice and
432 contributing to more accurate diagnoses. Currently, VLMs tailored for RG are predominantly utilized for
433 radiology images, with lesser application in other medical imaging domains such as pathology Sengupta
434 and Brown (2023), robotic surgery Xu et al. (2021), and ophthalmology Li et al. (2022).

435 3.5.2 Visual Question Answering (VQA)

436 VQA is another important visual-language understanding task, where the model needs to comprehend
437 images or videos and the posed question to provide a relevant and accurate response Antol et al. (2015).
438 The spectrum of questions encountered in VQA is broad, encompassing inquiries about the presence of
439 specific objects, their locations, or distinctive properties within the image. In the medical context Lin et al.
440 (2023b), this may involve questions regarding the presence of medical conditions or abnormalities, such
441 as “What abnormality is seen in the image?” Ionescu et al. (2021) or “Is there gastric fullness?” Lau et al.
442 (2018). Other queries may delve into details like the imaging method used Abacha et al. (2019), the organ
443 system involved Lau et al. (2018), or the presence of specific anatomical structures Liu et al. (2021a).

444 Questions in VQA fall into two categories. *Open-ended questions* elicit responses in the form of phrases or
445 sentences, fostering detailed and nuanced answers Thawkar et al. (2023). On the other hand, *closed-ended*
446 *questions* are designed to prompt limited responses, often with predetermined options, such as a short
447 list of multiple choices, a yes/no response, or a numeric rating Bazi et al. (2023). The task of VQA is
448 commonly approached as either a classification task, a generation task, or both Lin et al. (2023b). In the
449 classification approach, models select the correct answer from a predefined set, while in the generation
450 task, models produce free-form textual responses unconstrained by predefined options.

451 3.5.3 Other Tasks

452 Beyond VQA and RG, a spectrum of VLM tasks exist for the vision-language understanding Chen et al.
453 (2023). For instance, *referring expression comprehension* entails a model locating the specific area or object
454 in an image that the given phrase or sentence refers to Zhang et al. (2018). *Visual commonsense reasoning*
455 involves answering questions about an image, typically presented in a multiple-choice format, and justifying
456 the answer based on the model’s understanding of the image and common sense knowledge Zellers et al.
457 (2019). *Vision-language retrieval* focuses on either generating or retrieving relevant information from
458 images using textual data, or vice versa, obtaining information from text using visual data Zhen et al.
459 (2019). In the context of *visual captioning*, the model’s role is to generate a concise, text-based description
460 of either an image Sharma et al. (2023). It is worth highlighting that some of these tasks can seamlessly
461 transition from images to videos, showcasing the adaptability and versatility of VLMs across diverse visual
462 contexts Gan et al. (2022).

4 MEDICAL VLMS

463 4.1 Medical Datasets for VLMS

464 The adaptation of VLMs to various medical tasks is achieved through their pre-training and fine-tuning
465 using specialized task-specific datasets. Below is the list of vision-language datasets available in the public
466 domain that contain medical image-text pairs or question-answer (QA) pairs. Most of them are employed
467 by medical VLMs described in Section 4.3 for pre-training, fine-tuning, and evaluating VQA and RG tasks.

Table 1. A list of datasets used for developing medical VLMs. Datasets with image-text pairs are typically employed for training medical VLMs, as well as for fine-tuning and evaluating models on RG tasks. Additionally, datasets containing question-answer (QA) pairs are specifically designed for fine-tuning and evaluating models in VQA tasks.

Dataset	# image-text pairs	# QA pairs	Other components	Link
ROCO Pelka et al. (2018)	81,825	–	–	GH
MIMIC-CXR Johnson et al. (2019a)	377,110	–	–	PN
MIMIC-CXR-JPG Johnson et al. (2019b)	377,110	–	pathology labels	PN
MIMIC-NLE Kayser et al. (2022)	38,003	–	diagnosis labels, evidence labels	GH
CXR-PRO Ramesh et al. (2022)	–	–	374, 139 radiographs and 374, 139 reports but not paired	PN
MS-CXR Boecking et al. (2022)	1,162	–	bounding box annotations	PN
IU-Xray or Open-I Demner-Fushman et al. (2015)	7,470	–	labels	Web
MedICaT Subramanian et al. (2020)	224,567	–	annotations; inline references to ROCO figures	GH
PMC-OA Lin et al. (2023a)	1,650,000	–	–	HF
SLAKE Liu et al. (2021a)	–	14,028	642 annotated images, 5,232 medical triplets	Web
VQA-RAD Lau et al. (2018)	–	3,515	315 radiology images	Web
PathVQA He et al. (2020)	–	32,799	4,998 pathology images	GH
VQA-Med 2019 Abacha et al. (2019)	–	15,292	4,200 radiology images	GH
VQA-Med 2020 Abacha et al. (2020)	–	5,000	5,000 radiology images for VQA; images and questions for VQG	GH
VQA-Med 2021 Ionescu et al. (2021)	–	5,500	5,500 radiology images for VQA; images and questions for VQG	GH
EndoVis 2017 Allan et al. (2019)	–	472	bounding box annotations; 97 frames	GH
EndoVis 2018 Allan et al. (2020)	–	11,783	bounding box annotations; 2,007 frames	GH + Web
PathQABench-Public Lu et al. (2024b)	–	312	52 ROIs from WSIs	GH

Note: Abbreviations used are: GH - GitHub, HF - Hugging Face, and PN - PhysioNet

468 The comparative analysis of these datasets is presented in Table 1. Note that determining which dataset is
469 best suited for a particular task can be challenging, as each medical application presents its own nuances
470 and requirements. Factors such as the context in which images are acquired and the types of annotations
471 provided can significantly influence a dataset's effectiveness for specific tasks. In some cases, it may be

472 necessary to enhance existing datasets by adding relevant image-text pairs or QA pairs, or even to create
473 entirely new datasets tailored to specific research questions or clinical scenarios.

474 4.1.1 Radiology Objects in Context (ROCO)

475 ROCO is a dataset composed of image-caption pairs extracted from the open-access biomedical literature
476 database PubMed Central (PMC) Pelka et al. (2018). ROCO is stratified into two categories: radiology
477 and out-of-class. The radiology group includes 81,825 radiology images, including CT, ultrasound, x-ray,
478 fluoroscopy, positron emission tomography (PET), mammography, MRI, angiography, and PET-CT. The
479 out-of-class group has 6,127 images, including synthetic radiology images, clinical photos, portraits,
480 compound radiology images, and digital art. To facilitate model training, the dataset is randomly split into
481 a training set (65,460 radiology and 4,902 out-of-class images), a validation set (8,183 radiology and 612
482 out-of-class images), and a test set (8,182 radiology and 613 out-of-class images) using an 80/10/10 split
483 ratio, respectively.

484 4.1.2 Medical Information Mart for Intensive Care - Chest X-Ray (MIMIC-CXR)

485 MIMIC-CXR collection encompasses 377,110 chest X-rays paired with 227,835 associated free-text
486 radiology reports Johnson et al. (2019a). The dataset is derived from de-identified radiographic studies
487 conducted at the Beth Israel Deaconess Medical Center in Boston, MA. Each imaging study within the
488 MIMIC-CXR dataset consists of one or more images, typically featuring lateral and from back-to-front
489 (posteroanterior, PA) views in Digital Imaging and Communications in Medicine (DICOM) format.

490 4.1.3 MIMIC-CXR-JPG

491 MIMIC-CXR-JPG Johnson et al. (2019b) is a pre-processed variant of the MIMIC-CXR dataset Johnson
492 et al. (2019a). In this version, the original 377,110 images are converted into compressed JPG format. The
493 227,827 reports associated with these images are enriched with labels for various common pathologies.
494 The labels are derived from the analysis of the impression, findings, or final sections of the radiology
495 reports, facilitated by the use of NegBio Peng et al. (2017) and CheXpert (Chest eXpert) Irvin et al. (2019)
496 tools.

497 4.1.4 MIMIC-NLE

498 MIMIC-NLE dataset is specifically designed for the task of generating natural language explanations
499 (NLEs) to justify predictions made on medical images, particularly in the context of thoracic pathologies and
500 chest X-ray findings Kayser et al. (2022). The dataset consists of 38,003 image-NLE pairs or 44,935 image-
501 diagnosis-NLE triplets, acknowledging instances where a single NLE may explain multiple diagnoses.
502 NLEs are extracted from MIMIC-CXR Johnson et al. (2019a) radiology reports. The dataset exclusively
503 considers X-ray views from front-to-back (anteroposterior, AP) and back-to-front (posteroanterior, PA).
504 All NLEs come with diagnosis and evidence (for a diagnosis) labels. The dataset is split into the training
505 set with 37,016 images, a test set with 273 images, and a validation set with 714 images.

506 4.1.5 CXR with Prior References Omitted (CXR-PRO)

507 CXR-PRO dataset is derived from MIMIC-CXR Johnson et al. (2019a). The dataset consists of 374,139
508 free-text radiology reports containing only the impression sections Ramesh et al. (2022). It also incorporates
509 associated chest radiographs; however, the radiology reports and chest X-rays are not paired. This dataset
510 is designed to mitigate the problem of hallucinated references to prior reports often generated by radiology

511 report generation ML models. The omission of prior references in this dataset aims to provide a cleaner
512 and more reliable dataset for radiology RG.

513 4.1.6 Indiana University chest X-rays (IU-Xray)

514 IU-Xray dataset, also known as the *Open-I* dataset, is accessible through the National Library of
515 Medicine's Open-i service Demner-Fushman et al. (2015). The dataset originates from two hospital systems
516 within the Indiana Network for Patient Care database. This dataset comprises 7,470 DICOM chest X-rays
517 paired with 3,955 associated radiology reports. Indication, finding, and impression sections are manually
518 annotated using MeSH and RadLex (Radiology Lexicon) codes to represent clinical findings and diagnoses.
519 Throughout this review, we will refer to the dataset interchangeably as *IU-Xray* and *Open-I*, maintaining
520 consistency with the nomenclature used in related literature.

521 4.1.7 Medical Images, Captions, and Textual References (MedICaT)

522 MedICaT dataset contains 217,060 figures from 131,410 open-access PMC papers focused on radiology
523 images and other medical imagery types Subramanian et al. (2020). Excluding figures from ROCO Pelka
524 et al. (2018), the dataset integrates inline references from the S2ORC (Semantic Scholar Open Research
525 Corpus) Lo et al. (2020) corpus, establishing connections between references and corresponding figures.
526 Additionally, the inline references to ROCO figures are provided separately. MedICaT also contains 7,507
527 subcaption-subfigure pairs with annotations derived from 2,069 compound figures.

528 4.1.8 PubMedCentral's OpenAccess (PMC-OA)

529 PMC-OA dataset comprises 1.65 M image-caption pairs, derived from PMC papers Lin et al. (2023a). It
530 encompasses a variety of diagnostic procedures, including common ones such as ultrasound, MRI, PET,
531 and radioisotope, and rarer procedures like mitotic and fMRI. Additionally, the dataset covers a broad
532 spectrum of diseases, with induced cataracts, ear diseases, and low vision being among the most frequently
533 represented conditions.

534 4.1.9 MS-CXR

535 MS-CXR dataset contains image bounding box labels paired with radiology findings, annotated and
536 verified by two board-certified radiologists Boecking et al. (2022). The dataset consists of 1,162 image-
537 text pairs of bounding boxes and corresponding text descriptions. The annotations cover 8 different
538 cardiopulmonary radiological findings and are extracted from MIMIC-CXR Johnson et al. (2019a)
539 and REFLACX (Reports and Eye-tracking data For Localization of Abnormalities in Chest X-rays)
540 Bigolin Lanfredi et al. (2022) (based on MIMIC-CXR) datasets. The findings include atelectasis,
541 cardiomegaly, consolidation, edema, lung opacity, pleural effusion, pneumonia, and pneumothorax.

542 4.1.10 Semantically-Labeled Knowledge-Enhanced (SLAKE)

543 SLAKE is an English-Chinese bilingual dataset Liu et al. (2021a). It contains 642 images, including 12
544 diseases and 39 organs of the whole body. Each image is annotated with two types of visual information:
545 masks for semantic segmentation and bounding boxes for object detection. The dataset includes a total
546 of 14,028 QA pairs, categorized into vision-only or knowledge-based types and labeled accordingly,
547 encompassing both open- and closed-ended questions. Moreover, SLAKE incorporates 5,232 medical
548 knowledge triplets in the form of $\langle \text{head}, \text{relation}, \text{tail} \rangle$, where *head* and *tail* denote entities (e.g.,
549 organ, disease), and *relation* signifies the relationship between these entities (e.g., function, treatment).
550 An illustrative example of such a triplet is $\langle \text{pneumonia}, \text{location}, \text{lung} \rangle$.

551 4.1.11 VQA-RAD

552 VQA-RAD dataset contains 104 head axial single-slice CTs or MRIs, 107 chest x-rays, and 104 abdominal
553 axial CTs Lau et al. (2018). The images are meticulously chosen from MedPix, an open-access online
554 medical image database, ensuring each image corresponds to a unique patient. Furthermore, every selected
555 image has an associated caption and is deliberately devoid of any radiology markings. Every caption
556 provides details about the imaging plane, modality, and findings generated and reviewed by expert
557 radiologists. Also, VQA-RAD contains 3,515 QA pairs, with an average of 10 questions per image.
558 Among them, 1,515 are free-form questions and answers, allowing for unrestricted inquiry. Additionally,
559 733 pairs involve rephrased questions and answers, introducing linguistic diversity. Another 1,267 pairs are
560 framed, featuring questions presented in a structured format, offering consistency and systematic evaluation.
561 Additionally, QA pairs are split into 637 open-ended and 878 closed-ended types. Within the closed-ended
562 group, a predominant focus is on yes/no questions.

563 4.1.12 PathVQA

564 PathVQA is a dataset that encompasses 4,998 pathology images accompanied by a total of 32,799
565 QA pairs derived from these images He et al. (2020). The images are sourced from pathology books:
566 “Textbook of Pathology” and “Basic Pathology”, and the digital library “Pathology Education Informational
567 Resource”. Out of all QA pairs, 16,465 are of the open-ended type, while the remaining pairs are of the
568 closed-ended yes/no type. On average, each image is associated with 6.6 questions, which cover a broad
569 spectrum of visual contents, encompassing aspects such as color, location, appearance, shape, etc.

570 4.1.13 VQA-Med 2019

571 VQA-Med 2019 dataset contains 4,200 radiology images obtained from MedPix, an open-access online
572 medical image database, and 15,292 QA pairs Abacha et al. (2019). The training set consists of 3,200
573 images and 12,792 QA pairs, with each image having 3 to 4 associated questions. The validation set
574 includes 500 images and 2,000 QA pairs, and the test set comprises 500 images and 500 QA pairs. The
575 questions are mainly about modality, imaging plane, organ system, and abnormality.

576 4.1.14 VQA-Med 2020

577 VQA-Med 2020 dataset contains 5,000 radiology images obtained from MedPix, an open-access online
578 medical image database, and 5,000 QA pairs Abacha et al. (2020). The training set consists of 4,000
579 images and 4,000 QA pairs. The validation set comprises 500 images and 500 QA pairs, and the test set
580 includes 500 images and 500 QA pairs. The questions are focused on abnormalities present in the images.
581 Additionally, the dataset contains radiology images and questions for the Visual Question Generation
582 (VQG) task. The training set consists of 780 images and 2,156 associated questions. The validation set
583 comprises 141 images with 164 questions, and the test set includes 80 images.

584 4.1.15 VQA-Med 2021

585 VQA-Med 2021 dataset contains 5,500 radiology images obtained from MedPix, an open-access online
586 medical image database, and 5,500 QA pairs Ionescu et al. (2021). The training set consists of 4,500
587 images and 4,500 QA pairs. The validation set comprises 500 images and 500 QA pairs, and the test set
588 includes 500 images and 500 QA pairs. The questions are focused on abnormalities present in the images.
589 Similarly to VQA-Med 2019, the dataset also contains radiology images and questions for the VQG task.
590 The validation set comprises 85 images with 200 questions, and the test set includes 100 images.

591 4.1.16 Endoscopic Vision (EndoVis) 2017

592 EndoVis 2017 dataset contains 5 robotic surgery videos (two videos with 8 frames each, one with 18, one
 593 with 14, and one with 39 frames) from the MICCAI (Medical Image Computing and Computer Assisted
 594 Interventions) Endoscopic Vision 2017 Challenge Allan et al. (2019). It also includes 472 QA pairs with
 595 bounding box annotations. These QA pairs are carefully crafted to involve specific inquiries related to the
 596 surgical procedure. Examples of questions include queries such as "What is the state of prograsp forceps?"
 597 and "Where is the large needle driver located?". The inclusion of bounding box annotations enhances the
 598 dataset's utility for tasks such as object detection or answer localization.

599 4.1.17 EndoVis 2018

600 EndoVis 2018 dataset contains 14 robotic surgery videos (2,007 frames in total) from the MICCAI
 601 Endoscopic Vision 2018 Challenge Allan et al. (2020). It also includes 11,783 QA pairs regarding organs,
 602 surgical tools, and organ-tool interactions. When the question is about organ-tool interactions, the bounding
 603 box will contain both the organ and the tool.

604 4.1.18 PathQABench-Public

605 PathQABench-Public contains 52 regions of interest (ROIs) hand-selected by a board-certified pathologist
 606 from whole slide images (WSIs) in the publicly available The Cancer Genome Atlas (TCGA) repository.
 607 These images represent various organ systems: brain, lung, gastrointestinal tract, urinary tract, male
 608 reproductive tract, skin/eye/connective tissue, pancreaticohepatobiliary system, endocrine system,
 609 head/neck/mediastinum, gynecology, and breast. Per each organ system there are from 4 to 6 images. Each
 610 image is paired with a corresponding multiple-choice question, offering 10 possible answers. Additionally,
 611 there are five open-ended questions for each image, resulting in a total of 260 open-ended questions
 612 categorized into microscopy, diagnosis, clinical, and ancillary testing.

613 4.2 VLM Evaluation Metrics

614 This section delves into the evaluation process of medical VLMs. The initiation of this process involves
 615 meticulously selecting benchmark datasets and defining evaluation metrics tailored to the specific vision-
 616 language tasks at hand.

617 4.2.1 Evaluation Metrics for Report Generation

618 The prevalent benchmark datasets for medical RG are MIMIC-CXR Johnson et al. (2019a) and Open-I
 619 Demner-Fushman et al. (2015). For more information on these datasets, see Section 4.1. Several metrics
 620 are used to evaluate the effectiveness of VLMs on RG tasks. The more frequently used metrics are outlined
 621 below.

622 **Bilingual Evaluation Understudy (BLEU)** score was originally designed for machine translation
 623 evaluation, but it has been adapted for RG and even VQA in a modified form. BLEU provides a quantitative
 624 measure of how well the machine-generated text aligns with human-generated reference text Papineni et al.
 625 (2002). First, the precision of different *n*-grams, which are consecutive sequences of *n* words, is calculated
 626 using the formula:

$$\text{Precision}(n) = \frac{\#\text{overlapping n-grams}}{\#\text{all n-grams in a model-generated text}}, \quad (1)$$

627 where ‘overlapping n-grams’ refer to n-grams in the model-generated text that share common elements
 628 with at least one n-gram in the reference text. To ensure the precision score remains robust and is not
 629 disproportionately affected by repeated n-grams in the model-generated text, a modification known as
 630 clipping is often introduced. This process involves capping the count of each n-gram in the model-generated
 631 text to a maximum count. This maximum count is determined by the highest count observed in any single
 632 reference text for the same n-gram. The final BLEU-n score is defined as:

$$\text{BLEU-n} = BP \times \frac{1}{n} \exp \left(\sum_{k=1}^n \log [\text{Precision}(k)] \right). \quad (2)$$

633 In eq. 2, BP is referred to as the brevity penalty and is calculated as:

$$BP = \begin{cases} 1 & \text{if } c \geq r \\ e^{(1-r/c)} & \text{if } c < r, \end{cases} \quad (3)$$

634 where c is the length of the model-generated text, and r is the length of the reference text. It is common to
 635 use $n = 4$. The BLEU score ranges from 0 to 1, where a higher score suggests better agreement with the
 636 reference text. The overall BLEU score of the model is the average of BLEU scores for each pair of reports.

637 **Recall-Oriented Understudy for Gisting Evaluation (ROUGE)** is a set of metrics that evaluate the
 638 overlap between the model-generated text and human-generated reference text Lin (2004). ROUGE-n
 639 assesses the overlap of n-grams between model-generated text and reference text, and it is defined as:

$$\text{ROUGE-n} = \frac{\#\text{overlapping n-grams}}{\#\text{all n-grams in a reference text}}. \quad (4)$$

640 ROUGE-L focuses on measuring the longest common subsequence between model-generated text Y and
 641 reference text X , and it is calculated using the following relationship:

$$\text{ROUGE-L} = \frac{(1 + \beta^2) \times R \times P}{(R + P \times \beta^2)}, \quad (5)$$

642 where $R = \text{LCS}(X, Y)/m$, $P = \text{LCS}(X, Y)/n$, m is the length of X , n is the length of Y , $\text{LCS}(X, Y)$
 643 is the length of a longest common subsequence of X and Y , and β is a parameter that depends on the
 644 specific task and the relative importance of precision (P) and recall (R). There are other ROUGE score
 645 variants. The ROUGE scores range from 0 to 1, where higher scores indicate similarity between the
 646 model-generated text and the reference text. For each ROUGE variant, the overall score of the model is the
 647 average of scores for each instance.

648 **Metric for Evaluation of Translation with Explicit ORrdering (METEOR)** is an evaluation metric
 649 designed to be more forgiving than some other metrics and takes into account the fluency and meaning of
 650 the generated text Banerjee and Lavie (2005). The METEOR score is computed as follows:

$$\text{METEOR} = \frac{10 \times P \times R}{R + 9 \times P} (1 - \text{Penalty}) \quad (6)$$

651 where

$$R = \frac{\#\text{overlapping 1-grams}}{\#\text{1-grams in a reference text}}, \quad (7)$$

$$P = \frac{\#\text{overlapping 1-grams}}{\#\text{1-grams in a model-generated text}}, \quad (8)$$

$$\text{Penalty} = \frac{1}{2} \times \left(\frac{\#\text{chunks}}{\#\text{overlapping 1-grams}} \right)^3, \quad (9)$$

652 and *chunks* are groups of adjacent 1-grams in the model-generated text that overlap with adjacent 1-grams
 653 in the reference text. The METEOR score ranges from 0 to 1, with higher scores indicating better alignment
 654 between the model-generated text and the reference text. The overall METEOR score of a model is the
 655 average of scores for each instance.

656 **Perplexity** measures the average uncertainty of a model in predicting each word in a text Hao et al.
 657 (2020). The formula for perplexity is defined as:

$$\text{Perplexity} = \exp \left(-\frac{1}{n} \sum_{k=1}^n \ln P(w_k | w_1, w_2, \dots, w_{k-1}) \right), \quad (10)$$

658 where n is the total number of words in the text. The value of the perplexity metric can range from 1 to
 659 $+\infty$, and lower values signify a more accurate and confident model in capturing the language patterns
 660 within the given text.

661 **BERTScore** was initially designed for evaluating models that use BERT Devlin et al. (2019) embeddings
 662 Zhang et al. (2020). However, it can also leverage other word embeddings to evaluate the similarity between
 663 model-generated and reference text. The BERTScore of a single text pair is calculated according to the
 664 relationship:

$$\text{BERTScore} = \frac{2 \times P \times R}{P + R}, \quad (11)$$

665 where P represents the ratio of the maximum cosine similarity score between tokens in the model-generated
 666 text and the reference text to the numbers of tokens in the model-generated text and R represents the ratio
 667 of the maximum cosine similarity score between tokens in the model-generated text and the reference text
 668 to the numbers of tokens in the reference text. The BERTScore of the model is the average of BERTScores
 669 across all text pairs.

670 **RadGraph F1** is a novel metric that measures overlap in clinical entities and relations extracted from
 671 radiology reports Yu et al. (2023). The RadGraph F1 score is computed in the following way. First, the
 672 RadGraph model maps model-generated and reference reports into graph representations with clinical
 673 entities represented as nodes and their relations as edges between them. Second, the number of nodes that
 674 match between the two graphs based on clinical entity text and labels (entity type) is determined. Third,
 675 the number of edges that match between the two graphs based on their start and end entities and labels
 676 (relation type) is calculated. Lastly, the F1 score is separately computed for clinical entities and relations,
 677 and then the RadGraph F1 score for a report pair is the average of these two scores. The overall model
 678 performance is determined by averaging RadGraph F1 scores across all report pairs.

679 **Human evaluation** is crucial for assessing the quality of VLMs in medical RG. In Jeong et al. (2023),
 680 expert radiologists assessed the X-REM model's performance in RG by segmenting reports into lines and
 681 assigning scores based on five error categories to each line. These scores reflected error severity, with
 682 higher values indicating more severe errors.

683 The next few metrics are designed for classification evaluation, and RG can be viewed as such a task. In
 684 Moon et al. (2022), Lee et al. (2023), and Pellegrini et al. (2023), these metrics are computed based on the
 685 14 labels obtained from applying the CheXpert Irvin et al. (2019) or CheXbert Smit et al. (2020) labeler
 686 to the reference reports as well as the model-generated reports. In this context, reports bearing accurate
 687 diagnosis labels are categorized as positive, while those with inaccurate labels are regarded as negative.
 688 The following metrics are also called clinical efficacy metrics.

689 • *Accuracy* measures the ratio of all positive predictions to the total number of predictions.
 690 • *Precision* evaluates the accuracy of positive predictions. It is calculated as the ratio of true positive
 691 predictions to the total instances predicted as positive, expressed as:

$$\text{Precision} = \frac{\text{True Positives}}{\text{True Positives} + \text{False Positives}}. \quad (12)$$

692 High Precision indicates a low false positive rate.
 693 • *Recall* assesses the model's ability to predict all positive classes. It is defined as the ratio of correctly
 694 predicted positive observations to the total actual positives:

$$\text{Recall} = \frac{\text{True Positives}}{\text{True Positives} + \text{False Negatives}}. \quad (13)$$

695 High Recall means effectively identifying the most actual positive instances.
 696 • *F1 Score* provides an overall measure of the model's performance by balancing Precision and Recall.
 697 It is calculated as:

$$\text{F1} = \frac{2 \times \text{Precision} \times \text{Recall}}{\text{Precision} + \text{False Recall}}. \quad (14)$$

698 F1 scores range from 0 to 1, with higher values indicating better performance. In multi-class
 699 classification, the macro-F1 score is commonly computed by averaging the F1 scores independently
 700 calculated for each class. This method ensures unbiased evaluation across all classes, assigning equal
 701 importance regardless of size or prevalence.

702 4.2.2 Evaluation Metrics for VQA

703 The common benchmark datasets for medical VQA include VQA-RAD Lau et al. (2018), SLAKE Liu
 704 et al. (2021a), and PathVQA He et al. (2020). While various metrics are available for VQA evaluation,
 705 only a few are highlighted here to avoid redundancy with already mentioned metrics.

706 **Accuracy** is a fundamental metric for gauging overall model correctness in VQA evaluation. It is
 707 determined by calculating the proportion of correctly predicted answers to the total number of questions.
 708 For a detailed comparison of accuracies among different medical VLMs discussed in Section 4.3, refer to
 709 Table 3.

710 **Exact match** computes the ratio of generated answers that match exactly (excluding punctuation) the
711 correct answer. However, it may not credit semantically correct answers that lack an exact lexical match.
712 This metric is more suitable for evaluating answers to close-ended questions than open-ended ones.

713 **Human evaluation** can be performed for VQA in various ways. For instance, in Moor et al. (2023),
714 medical experts evaluated Med-Flamingo’s performance on each VQA problem using a user-friendly
715 interface, assigning scores from 0 to 10.

716 4.3 Medical Models

717 In this part of the review paper, we provide an overview of existing medical VLMs tailored for VQA
718 and/or RG. The information is organized chronologically based on the first appearance of the model. Our
719 focus is mainly on recently introduced open-source and publicly available models. A summary of these
720 VLMs is presented in Table 2.

721 4.3.1 Medical Vision Language Learner (MedViLL)

722 MedViLL can process medical images to generate associated reports Moon et al. (2022). The model
723 employs ResNet-50 He et al. (2016), trained on ImageNet Deng et al. (2009), for extracting visual features
724 v . The model leverages WordPiece Wu et al. (2016) tokenizer to extract textual features t from clinical
725 reports. Both visual and textual features incorporate positional information to capture spatial relationships
726 and sequential order. These features, along with special tokens $[CLS]$, $[SEP]_V$, $[SEP]_L$, are concatenated
727 into a single vector $(CLS, v, SEP_V, t, SEP_L)$ and fed into the BERT-based Transformer. The MedViLL
728 is pre-training on two tasks: MLM and ITM. The MLM task employs a bidirectional auto-regressive (BAR)
729 self-attention mask. For MLM, a negative log-likelihood loss function is used. Pre-training is performed
730 on 89,395 image-report pairs from MIMIC-CXR Johnson et al. (2019a), with fine-tuning on 3,547 pairs
731 from Open-I Demner-Fushman et al. (2015). VQA is performed on VQA-RAD Lau et al. (2018) (see Table
732 3), where the output representation of $[CLS]$ is used to predict a one-hot encoded answer. For radiology
733 RG fine-tuning, the model uses a sequence-to-sequence (S2S) mask instead of BAR and generates reports
734 by sequentially recovering MASK tokens. RG is evaluated on MIMIC-CXR Johnson et al. (2019a) and
735 Open-I Demner-Fushman et al. (2015). MedViLL achieves a BLEU-4 score of 0.066, a perplexity value of
736 4.185, and using a CheXpert labeler Irvin et al. (2019) an accuracy of 84.1%, a precision value of 0.698, a
737 recall value of 0.559, and an F1 score of 0.621 on MIMIC-CXR. Additionally, it achieves a BLEU-4 score
738 of 0.049, a perplexity value of 5.637, an accuracy of 73.4%, a precision value of 0.512, a recall value of
739 0.594, and an F1 score of 0.550 on Open-I.

740 4.3.2 PubMedCLIP

741 PubMedCLIP is a CLIP-based Radford et al. (2021) model pre-trained on the ROCO Pelka et al. (2018)
742 dataset Eslami et al. (2023). It employs a CLIP text encoder based on the Transformer architecture and three
743 distinct visual encoders: ViT-B/32 Dosovitskiy et al. (2021), ResNet-50, and ResNet-50 \times 4 He et al. (2016).
744 Following CLIP’s approach, the model generates joint representations by computing cosine similarity
745 between textual and visual features. The pre-training objective involves computing cross-entropy losses
746 for vision and language, which are then averaged to derive an overall loss. Repurposed as a pre-trained
747 visual encoder for VQA, PubMedCLIP’s output is also concatenated with the output of a convolutional
748 denoising autoencoder (CDAE) Masci et al. (2011). Questions are encoded using GloVe Pennington
749 et al. (2014) word embeddings followed by an LSTM Hochreiter and Schmidhuber (1997). Image and
750 question features are combined using *bilinear attention networks* (BAN) Kim et al. (2018), and the resulting
751 representations are classified using a two-layer feedforward neural network. The VQA loss combines

Table 2. A list of medical VLMs developed for VQA and RG.

Model	Stream	Decoder	Architecture	VQA	RG	Datasets	Code
MedViLL Moon et al. (2022)	single	No	RN50 + BERT	+	+	MIMIC-CXR, Open-I, VQA-RAD	GH
PubMedCLIP Eslami et al. (2023)	dual	No	ViT-B/32 or RN50 or RN50×4 + Transformer + BAN	+	-	ROCO, SLAKE, VQA-RAD	GH
RepsNet Tanwani et al. (2022)	dual	Yes	ResNeXt-101 + BERT + BAN + language decoder	+	+	VQA-RAD, IU-Xray	Web
BiomedCLIP Zhang et al. (2023a)	dual	No	ViT-B/16 + PubMedBERT + METER	+	-	PMC-15, SLAKE, VQA-RAD	HF
UniXGen Lee et al. (2023)	single	Yes	VQGAN + Transformer	-	+	MIMIC-CXR	GH
RAMM Yuan et al. (2023)	dual	No	Swiss Transformer + PubMedBERT + multimodal encoder w/ retrieval-atten. module	+	-	PMCPM, ROCO MIMIC-CXR, SLAKE, VQA-RAD, VQA-Med 2019, VQA-Med 2021	GH
X-REM Jeong et al. (2023)	dual	No	ALBEF (ViT-B/16 + BERT + multimodal encoder)	-	+	MIMIC-CXR, MedNLI, RadNLI	GH
Visual Med-Alpaca Shu et al. (2023)	single	Yes	DePlot or Med-GIT + prompt manager + LLaMa-7B	+	-	ROCO; MedDialog, MEDIQA QA, MEDIQA RQE, MedQA, PubMedQA + GPT-3.5-Turbo	GH
CXR-RePaiR-Gen Ranjit et al. (2023)	dual	Yes	ALBEF + FAISS retriever + prompt manager + text-davinci-003 or GPT-3.5-Turbo or GPT-4	-	+	CXR-PRO, MS-CXR	-
LLaVa-Med Li et al. (2023a)	single	Yes	ViT-L/14 + projection layer + LLaMa-7B	+	-	PMC-15 + GPT-4, VQA-RAD, SLAKE, PathVQA	GH
XrayGPT Thawkar et al. (2023)	single	Yes	MedCLIP + linear transformation layer + Vicuna-7B	+	+	MIMIC-CXR Open-I	GH
CAT-ViL DeiT Bai et al. (2023b)	dual	No	RN18 + CAT-ViL fusion module + DeiT	+	-	EndoVis 2017, EndoVis 2018	GH
MUMC Li et al. (2023b)	dual	Yes	ViT-B/12 + BERT + multimodal encoder + answer decoder	+	-	ROCO, MedICaT, ImageCLEF Caption, VQA-RAD, SLAKE PathVQA	GH
Med-Flamingo Moor et al. (2023)	single	Yes	ViT-L/14 + perceiver resampler + LLaMa-7B	+	-	MTB, PMC-OA, VQA-RAD, PathVQA, Visual USMLE	GH
RaDialog Pellegrini et al. (2023)	single	Yes	BioViL-T + BERT + prompt manager + Vicuna-7B	+	+	MIMIC-CXR, Instruct	GH
PathChat Lu et al. (2024b)	single	Yes	UNI + multimodal projector + Llama 2-13B	+	-	CONCH, PathChat dataset, PathQABench	GH

752 classification and image reconstruction losses. PubMedCLIP is fine-tuned on datasets like SLAKE Liu
753 et al. (2021a) and VQA-RAD Lau et al. (2018). Its performance is compared with existing Medical
754 VQA (MedVQA) methods, such as Mixture of Enhanced Visual Features (MEVF) Zhan et al. (2020)
755 and question-conditioned reasoning (QCR) Liu et al. (2023a). PubMedCLIP, integrated into the QCR

756 framework, achieves superior accuracies on VQA-RAD and SLAKE datasets compared to the MEVF
757 framework. The highest accuracies of PubMedCLIP in the QCR framework on both datasets are shown in
758 Table 3.

759 4.3.3 RepsNet

760 RepsNet is designed for VQA tasks Tanwani et al. (2022). It can generate automated medical reports
761 and interpret medical images. The model employs a modified version of the pre-trained ResNeXt-101 Xie
762 et al. (2016) as its image encoder and utilizes pre-trained BERT Devlin et al. (2019) as the text encoder,
763 with text tokenization done through WordPiece Wu et al. (2016). Fusion of image and question features
764 is achieved using BAN Kim et al. (2018). To align images with textual descriptions, the model employs
765 bidirectional contrastive learning Chen et al. (2020a). The language decoder, based on GPT-2, is adapted to
766 incorporate image features and prior context, generating text sequences in an auto-regressive manner until
767 an end-of-sequence token is produced. The overall loss function combines contrastive loss for encoding
768 phase and cross-entropy loss for decoding phase. For VQA tasks, the model is fine-tuned and evaluated on
769 VQA-RAD Lau et al. (2018) (see Table 3). In contrast, for RG, fine-tuning and evaluation are done using
770 IU-Xray Demner-Fushman et al. (2015) dataset. On the IU-Xray dataset, RepsNet achieves BLEU-2 and
771 BLEU-4 scores of 0.44 and 0.27, respectively.

772 4.3.4 BiomedCLIP

773 BiomedCLIP is pre-trained on the specifically curated PMC-15 dataset that consists of 15 M figure-
774 caption pairs derived from the PMC articles Zhang et al. (2023a) but is not publicly available. The
775 model architecture is similar to CLIP Radford et al. (2021), except that the text encoder is a pre-trained
776 PubMedBERT Gu et al. (2021) model with WordPiece tokenizer Wu et al. (2016). The model uses ViT-B/16
777 Dosovitskiy et al. (2021) as the visual data encoder. For pre-training, the model adopts the CL approach,
778 and to mitigate memory usage, it utilizes the sharding contrastive loss Cherti et al. (2022). For adaptation
779 to VQA, the model incorporates the METER Dou et al. (2022) framework. This involves deploying a
780 Transformer-based co-attention multimodal fusion module that produces cross-modal representations.
781 These representations are then fed into a classifier for the final prediction of answers. The model is
782 evaluated on VQA-RAD Lau et al. (2018) and SLAKE (English) Liu et al. (2021a) datasets (see Table 3).

783 4.3.5 Unified chest X-ray and report Generation model (UniXGen)

784 UniXGen is a unified model that can generate both reports and view-specific X-rays Lee et al. (2023).
785 The model tokenizes chest X-rays leveraging VQGAN Esser et al. (2021), a generative model that
786 amalgamates generative adversarial networks (GANs) with vector quantization (VQ) techniques. VQGAN
787 employs an encoder to transform input images into continuous representations, subsequently using vector
788 quantization to discretize them into learnable codebook vectors. Additionally, VQGAN incorporates a
789 decoder, translating these discrete codes back into images during the generation process. For chest X-rays,
790 multiple views from the same study are tokenized into sequences of discrete visual tokens, demarcated
791 by special tokens to distinguish perspectives. In the case of radiology reports, the model uses the byte-
792 level BPE Wang et al. (2020) tokenizer, augmented with sinusoid positional embedding for enhanced
793 representation. The model is based on the Transformer architecture Vaswani et al. (2017) with a multimodal
794 causal attention mask, ensuring that each position in the sequence attends to all previous positions and
795 not future ones. During training, multiple views of chest X-rays and a report embedding are concatenated
796 randomly and fed into the Transformer. The model is optimized using the negative log-likelihood loss
797 function. The model is trained on 208,534 studies sampled from the MIMIC-CXR Johnson et al. (2019a)

798 dataset. Each study contains at most three chest X-rays representing PA (from back to front), AP (from
799 front to back), and lateral views. On the MIMIC-CXR dataset, UniXGen achieves a BLEU-4 score of
800 0.050 and, using the CheXpert labeler Irvin et al. (2019), attains a precision score of 0.431, a recall value
801 of 0.410, and an F1 score of 0.420.

802 4.3.6 Retrieval-Augmented bioMedical Multi-modal Pretrain-and-Finetune Paradigm (RAMM)

803 RAMM, a retrieval-augmented VLM designed for biomedical VQA, integrates Swin Transformer Liu
804 et al. (2021b) as its image encoder and PubMedBERT Gu et al. (2021) as its text encoder Yuan et al. (2023).
805 The visual and textual features are then fused by the multimodal encoder, a 6-layer Transformer Vaswani
806 et al. (2017). The model is pre-trained on the MIMIC-CXR Johnson et al. (2019a) and ROCO Pelka et al.
807 (2018) datasets along with a newly curated PMC-Patients-Multi-modal (PMCPM) dataset, consisting of
808 398,000 image-text pairs sampled from PMC-OA Lin et al. (2023a) dataset. The pre-training objective
809 function of RAMM is the sum of three tasks: CL, ITM, and MLM. Using CL, the model aligns images and
810 texts using the cosine similarity metric. The VQA task is viewed as a classification problem, and the model
811 is optimized using the cross-entropy loss function. During model fine-tuning, the retrieval-attention module
812 fuses the representations of the image-question input with four representations of the retrieved image-text
813 pairs from the pre-trained datasets. This lets RAMM to focus on relevant parts of the retrieved information
814 when generating answers. The model is evaluated on VQA-Med 2019 Abacha et al. (2019), VQA-Med
815 2021 Ionescu et al. (2021), VQA-RAD Lau et al. (2018), and SLAKE Liu et al. (2021a) datasets (see Table
816 3).

817 4.3.7 Contrastive X-Ray REport Match (X-REM)

818 X-REM is a retrieval-based radiology RG model that uses an ITM score to measure the similarity of a
819 chest X-ray image and radiology report for report retrieval Jeong et al. (2023). The VLM backbone of
820 the model is ALBEF Li et al. (2021). ALBEF utilizes ViT-B/16 Dosovitskiy et al. (2021) as its image
821 encoder and initializes the text encoder with the first 6 layers of the BERT Devlin et al. (2019) base model.
822 The multimodal encoder in ALBEF, responsible for combining visual and textual features to generate
823 ITM scores, is initialized using the final six layers of the BERT base model. X-REM leverages ALBEF's
824 pre-trained weights and performs further pre-training on X-rays paired with extracted impression sections
825 (2,192 pairs), findings sections (1,597 pairs), or both (2,192 pairs) from the MIMIC-CXR Johnson et al.
826 (2019a) dataset. Subsequently, the model is fine-tuned on the ITM task, where the scoring mechanism
827 involves using the logit value for the positive class as the similarity score for image-text pairs. To address
828 the positive skewness in medical datasets, 14 clinical labels obtained from the CheXbert Smit et al. (2020)
829 labeler are utilized. The model efficiently manages the computational burden associated with ITM scores
830 by employing ALBEF's pre-aligned unimodal embeddings. This involves narrowing down the candidate
831 reports based on high cosine similarity with the input image before computing ITM scores. Additionally,
832 the text encoder undergoes fine-tuning on natural language inference (NLI) task, utilizing datasets such as
833 MedNLI Romanov and Shivade (2018) and RadNLI Miura et al. (2021). This step is crucial for preventing
834 the retrieval of multiple reports with overlapping or conflicting information. X-REM achieves a BLEU-2
835 score of 0.186 on the MIMIC-CXR (Findings only) dataset. The BERTScore of the model is 0.386 on
836 MIMIC-CXR (Findings only) and 0.287 on MIMIC-CXR (Impressions and Findings).

837 4.3.8 Visual Med-Alpaca

838 Visual Med-Alpaca is a biomedical FM designed for addressing multimodal biomedical tasks like VQA
839 Shu et al. (2023). The model processes image inputs through a classifier to select the appropriate module for

840 converting visual information into text, with supported modules including DePlot Liu et al. (2022) for plots
841 and Med-GIT Wang et al. (2022a) fine-tuned on the ROCO Pelka et al. (2018) dataset for radiology images.
842 The prompt manager combines textual information from images and text inputs to form prompts for the
843 LLaMA-7B Touvron et al. (2023a) model. However, before generating responses, LLaMA-7B undergoes
844 both standard and LoRA Hu et al. (2022) fine-tuning on a carefully curated set of 54,000 medical QA
845 pairs. The questions within this set are derived from question-answering datasets such as MEDIQA QA
846 Ben Abacha et al. (2019), MEDIQA RQE Ben Abacha et al. (2019), MedQA Jin et al. (2021), MedDialog
847 Zeng et al. (2020), and PubMedQA Jin et al. (2019), with their corresponding answers synthesized using
848 GPT-3.5-Turbo in the *self-instruct* Wang et al. (2023b) manner. Human experts filter and edit the obtained
849 QA pairs for quality and relevance. The evaluation of this model is still ongoing Shu et al. (2023).

850 4.3.9 Contrastive X-ray-Report Pair Retrieval based Generation (CXR-RePaiR-Gen)

851 CXR-RePaiR-Gen, designed for radiology RG, integrates the RAG framework to address hallucinated
852 references Ranjit et al. (2023). The model leverages the pre-trained ALBEF Li et al. (2021) previously
853 utilized in CXR-ReDonE Ramesh et al. (2022). Textual features are indexed in a vector database, Facebook
854 AI Similarity Search (FAISS). When given a radiology image input, embeddings from the reports or
855 sentences corpus with the highest dot-product similarity to the image embedding are retrieved. The CXR-
856 PRO Ramesh et al. (2022) dataset is employed for text retrieval to gather relevant impressions for generating
857 the radiology report. The retrieved impression sections from the CXR-PRO dataset serve as the context for
858 the prompt to an LLM, along with instructions to generate the radiology report. Two prompts are employed:
859 one for the text-davinci-003 model and another for conversational RG with GPT-3.5-Turbo and GPT-4
860 models. The model is evaluated on MS-CXR Boecking et al. (2022) and CXR-PRO datasets. A code has
861 yet to be provided for this model. Evaluated on MS-CXR and CXR-PRO datasets, CXR-RePaiR-Gen
862 achieves BERTScore scores of 0.2865 on CXR-PRO (GPT-4) and 0.1970 on MS-CXR (text-davinci-003).
863 Its RadGraph F1 scores are 0.1061 on CXR-PRO (GPT-4) and 0.0617 on MS-CXR (text-davinci-003),
864 employing three retrieval samples per input during RAG.

865 4.3.10 Large Language and Vision Assistant for BioMedicine (LLaVa-Med)

866 LLaVa-Med, an adaptation of LLaVa Liu et al. (2023c), is customized for the medical domain through
867 training on instruction-following datasets Li et al. (2023a). Visual features are extracted by the pre-trained
868 CLIP visual encoder ViT-L/14 Dosovitskiy et al. (2021), which can be substituted with BiomedCLIP
869 Zhang et al. (2023a). These features are mapped into textual embedding space via linear projection layer
870 and combined with instructions before being input to the LLM LLaMA-7B Touvron et al. (2023a), which
871 can be replaced with Vicuna Chiang et al. (2023). After initializing with the general-domain LLaVA, the
872 model undergoes fine-tuning using curriculum learning. First, the model learns to connect visual elements
873 in biomedical images to corresponding language descriptions, using a dataset of 600,000 image-caption
874 pairs from PMC-15, initially employed in BiomedCLIP. These image-caption pairs are transformed into an
875 instruction-following dataset, where the instructions prompt the model to describe the corresponding image
876 concisely or in detail. Given the language instruction and image input, the model is prompted to predict the
877 original caption. The visual encoder and language model weights are frozen during this stage, with updates
878 exclusively applied to the linear projection layer. The second stage of training focuses on aligning the
879 model to follow diverse instructions. For this purpose, another instruction-following dataset is generated
880 from PMC-15. Instructions for this dataset are designed to guide the GPT-4 model to generate multi-round
881 questions and answers from the image caption and sentences from the original PMC paper mentioning the
882 image Li et al. (2023a). In this training phase, the model undergoes training on a set of 60,000 images, each

883 accompanied by its respective caption and multi-round questions and answers. Throughout this process,
884 the weights of the visual encoder remain unchanged, preserving the previously acquired visual features.
885 Meanwhile, the pre-trained weights of the projection layer and the language model undergo continuous
886 updates. Lastly, for VQA, the model is fine-tuned and evaluated on VQA-RAD Lau et al. (2018), SLAKE
887 Liu et al. (2021a), and PathVQA He et al. (2020) (see Table 3).

888 4.3.11 XrayGPT

889 XrayGPT is a conversational medical VLM specifically developed for analyzing chest radiographs
890 Thawkar et al. (2023). The VLM uses MedCLIP Wang et al. (2022b) to generate visual features. These
891 features undergo a meticulous transformation process: initially, they are mapped to a lower-dimensional
892 space through a linear projection head and subsequently translated into tokens via a linear transformation
893 layer. The model incorporates two text queries: an assistant query framing its purpose and a doctor's query
894 guiding relevant information provision. Tokens generated from a visual input are concatenated with the
895 tokenized queries and then fed into Vicuna-7B Chiang et al. (2023), fine-tuned on 100,000 patient-doctor
896 and 20,000 radiology conversations sourced from ShareGPT .com. During training, the weights of the
897 vision encoder and LLM are frozen while the weights of the linear transformation layer undergo updates.
898 The model is first trained on 213,514 image-text pairs from pre-processed MIMIC-CXR Johnson et al.
899 (2019a) dataset and then on 3,000 image-text pairs from Open-I Demner-Fushman et al. (2015) dataset.
900 XrayGPT achieves ROUGE-1 = 0.3213, ROUGE-2 = 0.0912, and ROUGE-L = 0.1997 on MIMIC-CXR
901 dataset.

902 4.3.12 Co-Attention gaTed Vision-Language Data-efficient image Transformer (CAT-ViL DeiT)

903 CAT-ViL DeiT is a specialized VLM tailored for VQA within surgical scenarios, focusing on answer
904 localization Bai et al. (2023b). It integrates ResNet-18 He et al. (2016) pre-trained on ImageNet Deng et al.
905 (2009) to generate visual features and custom BERT tokenizer Seenivasan et al. (2022) for text encoding.
906 The *Co-Attention gaTed Vision-Language* (CAT-ViL) module facilitates interaction between visual and
907 textual features, fused via gating mechanisms to optimize multimodal embeddings. These embeddings
908 are further processed by a pre-trained *Data-efficient image Transformer* (DeiT) module for optimal joint
909 representation. For VQA, the model adopts a standard classification head, while for answer localization
910 within images, it employs the *detection with transformers* (DETR) Carion et al. (2020) head. The overall
911 loss function comprises cross-entropy as the classification loss and L1-norm, along with the *generalized*
912 *intersection over union* (GIoU) Rezatofighi et al. (2019), serving as the localization loss. The model is
913 trained on 1,560 frames, and 9,014 QA pairs from the surgical datasets EndoVis 2018 Allan et al. (2020).
914 The model achieved an accuracy of 61.92% on the remaining data from EndoVis 2018 and 45.55% on
915 EndoVis 2017 Allan et al. (2019) dataset.

916 4.3.13 Masked image and text modeling with Unimodal and Multimodal Contrastive losses 917 (MUMC)

918 MUMC utilizes a ViT-B/12 Dosovitskiy et al. (2021) as its image encoder, the first 6 layers of BERT
919 Devlin et al. (2019) as its text encoder, and the last 6 layers of BERT as its multimodal encoder Li et al.
920 (2023b). The multimodal encoder incorporates cross-attention layers to align visual and textual features.
921 For pre-training, the model employs CL, MLM, and ITM. Also, the model utilizes a newly introduced
922 *masked image strategy*, randomly masking 25% of image patches as a data augmentation technique. This
923 exposes the model to a greater variety of visual contexts and enables learning representations that are more
924 robust to partially occluded inputs. The pre-training is performed on ROCO Radford et al. (2021), MediCaT

925 Subramanian et al. (2020), and Image Retrieval in Cross-Language Evaluation Forum (ImageCLEF) caption
926 Rückert et al. (2022) datasets. For VQA tasks, an answering decoder is added to generate answer text
927 tokens. The encoder weights are initialized from pre-training, and the model is fine-tuned and evaluated on
928 VQA-RAD Lau et al. (2018), SLAKE Liu et al. (2021a), and PathVQA He et al. (2020) (see Table 3).

929 4.3.14 Med-Flamingo

930 Med-Flamingo is a multimodal few-shot learner model based on the Flamingo Alayrac et al. (2022)
931 architecture, adapted to the medical domain Moor et al. (2023). The model is pre-trained on the MTB
932 Moor et al. (2023) dataset, a newly curated collection comprising 4,721 segments from various Medical
933 TextBooks, encompassing textual content and images. Each segment is designed to contain at least one
934 image and up to 10 images, with a specified maximum length. Also, it is pre-trained on 1.3 M image-caption
935 pairs from the PMC-OA Lin et al. (2023a) dataset. The model's few-shot capabilities are achieved through
936 training on these mixed text and image datasets, enabling it to generalize and perform diverse multimodal
937 tasks with only a few examples. The model utilizes a pre-trained frozen CLIP vision encoder ViT-L/14 for
938 visual feature generation. To convert these visual features into a fixed number of tokens, the model employs
939 a module known as the *perceiver resampler*, which is trained from scratch. Subsequently, these tokens and
940 tokenized text inputs undergo further processing in a pre-trained frozen LLM LLaMA-7B Touvron et al.
941 (2023a), enhanced with gated cross-attention layers, which are trained from scratch. This augmentation aids
942 in learning novel relationships and enhances training stability. Med-Flamingo's performance is evaluated
943 on VQA-RAD Lau et al. (2018) and PathVQA He et al. (2020). The exact match scores for MedFlamingo
944 demonstrate a few-shot performance of 0.200 on VQA-RAD and 0.303 on PathVQA. In contrast, the zero-
945 shot performance yields an exact match score of 0.000 on VQA-RAD and 0.120 on PathVQA. Additionally,
946 it is evaluated on a specifically created Visual United States Medical Licensing Examination (USMLE)
947 dataset, comprising 618 challenging open-ended USMLE-style questions augmented with images, case
948 vignettes, and tables of laboratory measurements, covering a diverse range of medical specialties.

949 4.3.15 RaDialog

950 RaDialog is a VLM that integrates automated radiology RG with conversational assistance Pellegrini et al.
951 (2023). The model incorporates BioViL-T Bannur et al. (2023), a hybrid model that fuses the strengths of
952 ResNet-50 He et al. (2016) and Transformer Vaswani et al. (2017) architectures. Pre-trained on radiology
953 images and reports, BioViL-T generates patch-wise visual features. The extracted features undergo
954 alignment through a BERT Devlin et al. (2019) model, transforming them into a concise representation of
955 32 tokens. The model incorporates the CheXpert classifier to offer organized findings in medical images.
956 These findings are generated based on labels obtained from the CheXbert Smit et al. (2020) model. The
957 classifier is trained independently using labels predicted by CheXbert from the findings section of radiology
958 reports. Visual features, structured findings, and a directive prompt are combined as input for the Vicuna-7B
959 LLM, fine-tuned using LoRA. The training is performed on MIMIC-CXR Johnson et al. (2019a) dataset.
960 RaDialog achieves a BLEU-4 score of 0.095, ROUGE-L score of 0.2710, METEOR score of 0.14, and
961 BERTScore of 0.400 on the MIMIC-CXR dataset. To address the challenge of catastrophic forgetting during
962 training and ensure the model's capability across diverse downstream tasks, it is specifically trained on the
963 newly created Instruct Pellegrini et al. (2023) dataset. This dataset is meticulously curated to encompass
964 a spectrum of 8 diverse tasks: RG, NLE, complete CheXpert QA, binary CheXpert QA, region QA,
965 summarization, report correction, and reformulation report using simple language. Carefully formulated
966 prompts accompany each task, tailored to elicit specific responses from the model. For instance, some
967 prompts involve answering questions about particular X-ray regions. RaDialog trained on the Instruct

Table 3. The comparison of medical VLMs' accuracies on VQA tasks. The underlined accuracies are the highest for a specific dataset.

Model	SLAKE open -ended	SLAKE close -ended	VQA-RAD open -ended	VQA-RAD close -ended	PathVQA open -ended	PathVQA close -ended	VQA-Med 2019	VQA-Med 2021
MedViLL Moon et al. (2022)	–	–	59.50%	77.70%	–	–	–	–
PubMedCLIP Eslami et al. (2023)	78.40%	82.50%	60.10%	80.00%	–	–	–	–
RepsNet Tanwani et al. (2022)	–	–	–	<u>87.05%</u>	–	–	–	–
BioMedCLIP Zhang et al. (2023a)	<u>82.50%</u>	89.70%	67.60%	79.80%	–	–	–	–
RAMM Yuan et al. (2023)	82.48%	<u>91.59%</u>	67.60%	85.29%	–	–	<u>82.13%</u>	<u>39.20%</u>
LLaVa-Med Li et al. (2023a)	–	84.19%	–	85.34%	–	<u>91.21%</u>	–	–
MUMC Li et al. (2023b)	–	–	<u>71.50%</u>	84.20%	<u>39.00%</u>	90.4%	–	–

968 dataset achieves an F1 score of 0.397 on the binary CheXpert QA task and 0.403 on the complete CheXpert
 969 QA task. In contrast, RaDialog without being trained on Instruct achieves lower F1 scores of 0.018 and
 970 0.098, respectively.

971 4.3.16 PathChat

972 PathChat is a multimodal generative AI copilot designed for human pathology Lu et al. (2024b). It
 973 employs UNI Chen et al. (2024), built on the ViT-L backbone and pre-trained using SSL on over 100 M
 974 histology image patches from approximately 100,000 WSIs, to generate visual features. PathChat uses
 975 the Llama 2 13B Touvron et al. (2023b) LLM for text decoding, which is pre-trained on general text
 976 data. The UNI is connected to the LLM through a multimodal projector that maps visual tokens into
 977 the LLM's embedding space. During PathChat's pre-training phase, UNI and multimodal projector are
 978 trained on the CONCH Lu et al. (2024a) dataset, comprising 1.18 M pathology image-caption pairs sourced
 979 from PMC-OA Lin et al. (2023a) and internally curated datasets, aligning the image representations with
 980 pathology text while keeping the LLM weights frozen. The whole dataset is not publicly available. During
 981 instruction fine-tuning, the entire model is trained end-to-end on a specially curated PathChat dataset
 982 consisting of 456,916 pathology-specific instructions of 6 different types and 999,202 QA pairs. The model
 983 is evaluated on the newly curated PathQABench dataset, consisting of public and private subparts. On the
 984 multiple-choice questions across the entire PathQABench dataset, PathChat achieved an accuracy of 78.1%
 985 when only images and questions are provided to the model and 89.5% when clinical data is also included.
 986 For open-ended questions, PathChat attained an accuracy of 78.7% on the subset of questions for which
 987 pathologist evaluators reached a consensus.

5 CHALLENGES AND FUTURE DIRECTIONS

988 As VLMs become more prevalent in healthcare, various challenges and opportunities for future research
989 emerge. This section highlights key obstacles and proposes research directions to improve VLM's
990 effectiveness and seamless integration within clinical environments.

991 5.1 Data Availability and Privacy

992 A significant challenge in developing effective medical VLMs is the limited availability of ML-ready
993 diverse and representative medical datasets. This limitation restricts the comprehensive training of VLMs,
994 impeding their ability to understand the complexities of diverse and rare clinical scenarios Moor et al.
995 (2023). To mitigate privacy concerns, most datasets undergo rigorous pre-processing to remove Protected
996 Health Information (PHI) before model training. The common approach is using algorithms to detect and
997 remove sensitive information from structured and unstructured data. For example, Philter redacts PHI from
998 clinical notes Norgeot et al. (2020). ImageDePHI automates the removal of PHI from WSIs Clunie et al.
999 (2024). Another approach is replacing identifying information with artificial identifiers, which keeps data
1000 linkable without disclosing personal details. However, the risk of PHI leakage still remains a concern.

1001 In the future, addressing this limitation can involve employing innovative approaches such as RAG
1002 and federated learning (FL). While RAG usually involves a frozen model during training, exploring the
1003 pre-training of VLMs within the RAG framework opens up a new avenue of research Zhao et al. (2023).
1004 This innovative approach can potentially enhance the robustness of VLMs, especially in handling new
1005 and unforeseen medical cases. Additionally, FL offers a promising strategy to address data scarcity while
1006 protecting patient privacy Zhang et al. (2021). In FL, models are trained locally at multiple institutions
1007 on their own patient data. Each institution shares the updated model weights with the central server. The
1008 server then aggregates these weights to create a global model. Later, the updated global model can be sent
1009 back to institutions for fine-tuning. To further safeguard privacy, the weights in FL can be protected using
1010 techniques such as differential privacy (DP) or homomorphic encryption (HE). In DP, noise is added to the
1011 gradients before they are sent to the central server Dwork (2006). In contrast, HE encrypts the weights,
1012 allowing the central server to perform computations on them without decryption Stripelis et al. (2021).
1013 Future research can focus on optimizing the balance between privacy and performance of VLMs, and
1014 enhancing the efficiency of encryption methods in FL Koutsoubis et al. (2024b,a).

1015 5.2 Proper Evaluation Metrics

1016 In medical RG, traditional metrics like BLEU and ROUGE can be used to effectively quantify surface-
1017 level linguistic similarity by capturing text overlap and structural matching between generated and reference
1018 texts. METEOR goes further by accounting for synonyms and stemming, providing a more nuanced view
1019 of textual similarities. Perplexity, often used to measure language fluency, evaluates how well the generated
1020 text adheres to natural language patterns. Together, these metrics assess fluency, coherence, and overall
1021 readability, ensuring that generated reports are well-formed and comprehensible. However, they often
1022 fall short in capturing the nuanced complexities of clinical language and contextual relevance critical in
1023 medical settings Yu et al. (2023). Specifically, they may fail to determine whether a report accurately
1024 conveys essential clinical findings or diagnoses. Advanced metrics like BERTScore seek to assess semantic
1025 similarity beyond surface-level text overlap, but they require fine-tuning on medical datasets to understand
1026 specialized terminology and relationships, and may still miss subtle clinical nuances.

1027 In medical VQA, traditional metrics like Accuracy, Precision, and Recall are commonly used to evaluate
1028 how well VLMs answer clinical questions, such as identifying medical conditions or anatomical features.

1029 While these metrics effectively assess binary outcomes, they fail to account for the varying clinical relevance
1030 or significance of errors made by the model. For example, misclassifying a serious condition may have
1031 far more severe consequences than making minor prediction errors, yet this distinction is not captured in
1032 simple accuracy-based evaluations.

1033 To address the limitations of traditional metrics, it is imperative to develop specialized metrics tailored
1034 for medical RG and VQA, particularly for open-ended medical queries. For instance, RadGraph F1 Yu
1035 et al. (2023) was developed to evaluate the extraction of clinical entities (e.g., diagnoses, findings) and their
1036 relations (e.g., linking conditions to anatomical locations) in radiology reports. This metric is particularly
1037 valuable for assessing structured medical data, ensuring that reports capture not only relevant clinical
1038 entities but also their correct relationships, which is crucial for the accuracy and integrity of medical
1039 conclusions. The development of additional specialized metrics is vital for evaluating VLMs performance
1040 and for assessing factors such as generalization, efficiency, and robustness in clinical decision-making and
1041 diagnostic support. Furthermore, integrating these metrics with other quantitative measures and human
1042 assessments can significantly enhance evaluations and drive continuous advancements in the capabilities of
1043 medical VLMs.

1044 5.3 Hallucinations

1045 The issue of hallucinations in generative VLMs poses a significant challenge to their reliability and
1046 practical application Liu et al. (2024). Hallucinations refer to instances where VLMs generate outputs
1047 that are not grounded in the provided images or inconsistent with the established knowledge. In medical
1048 contexts, these hallucinations can have serious consequences, leading to inaccurate diagnostic information
1049 or treatment recommendations. One identified cause of hallucinations is the lack of alignment between
1050 visual and textual information Sun et al. (2023). Training VLMs to effectively align these data modalities
1051 is crucial in mitigating the risk of hallucinations. For instance, LLaVA-RLHF Sun et al. (2023) achieved
1052 hallucination reduction by incorporating RLHF to align different modalities. Further research can focus
1053 on integrating RLHF into medical VLMs. Additionally, incorporating RAG can help reduce the risk of
1054 generating misleading or fabricated outputs by allowing the system to analyze medical images while
1055 simultaneously accessing relevant information from trusted textual sources.

1056 5.4 Catastrophic Forgetting

1057 Overcoming catastrophic forgetting poses an additional challenge in the development of medical VLMs.
1058 Catastrophic forgetting occurs when a model learns new information but inadvertently erases or distorts
1059 previously acquired knowledge, potentially compromising its overall competence. Striking a balance during
1060 fine-tuning can be crucial; moderate fine-tuning can be helpful to adapt the model to a specific task, while
1061 excessive fine-tuning can lead to catastrophic forgetting Zhai et al. (2023); Khan et al. (2023). As a future
1062 research direction, leveraging methodologies from continual learning Wang et al. (2023a); Zhou et al.
1063 (2023a); Cai and Rostami (2024); Khan et al. (2023, 2024) might be useful in the context of medical VLMs.
1064 Continual learning focuses on training models to sequentially learn from and adapt to new data while
1065 retaining knowledge from previously encountered tasks Khan et al. (2024). Also, incorporating adapters
1066 within the framework of continual learning can be a valuable tool in mitigating catastrophic forgetting
1067 Zhang et al. (2023b).

1068 **5.5 Integration into Hospital Systems**

1069 Integrating VLMs into hospital systems also presents substantial challenges, requiring extensive
1070 collaboration between medical professionals and AI/ML researchers. First, medical professionals must
1071 maintain rigorous data collection practices to ensure that the data is clean, well-organized, and accessible,
1072 as ML experts rely on high-quality data to train and fine-tune VLMs. Second, VLMs must be designed
1073 to address the right clinical questions, ensuring their relevance and utility in medical practice. Third,
1074 healthcare professionals need training to use VLMs effectively, and the models should be intuitive and
1075 user-friendly to integrate smoothly into daily clinical routines. **Furthermore**, implementation scientists play
1076 a crucial role in this process by facilitating collaboration between clinicians and ML experts Reddy (2024).
1077 They help bridge the gap between these two groups, ensuring that VLMs are both technically robust and
1078 clinically relevant.

1079 In this context, models like RaDialog Pellegrini et al. (2023) and PathChat Lu et al. (2024b) show the
1080 potential of VLMs to enhance clinical effectiveness. RaDialog demonstrates a solid capability to produce
1081 clinically accurate radiology reports. It transforms static reporting into a dynamic tool where clinicians can
1082 ask follow-up questions and seamlessly incorporate expert insights. This aligns closely with the interactive
1083 processes typical in clinical settings. Meanwhile, PathChat demonstrates promising clinical effectiveness
1084 as an AI copilot for pathology. It can assist pathologists in their work in real medical settings, including
1085 human-in-the-loop clinical decision-making, complex diagnostic workups, analyzing morphological details
1086 in histology images, and guiding immunohistochemistry (IHC) interpretations. However, the assessment of
1087 VLM effectiveness in medical environments is an open research question. Comprehensive clinical trials are
1088 necessary to confirm that VLMs truly enhance patient care and integrate effectively into existing clinical
1089 workflows.

1090 **5.6 Security**

1091 The security of VLMs must be thoroughly considered, focusing on privacy, minimizing medical errors,
1092 and preventing the introduction of significant new errors. VLMs must be kept behind the hospital
1093 firewall to protect sensitive medical information. It is also crucial to involve independent experts in
1094 the validation process. Validating the model on unseen medical data can help identify and rectify potential
1095 inaccuracies. **Additionally**, adversarial attacks represent another significant security issue, as they can
1096 exploit vulnerabilities in the model, leading to incorrect predictions. To combat this, incorporating
1097 adversarial training by exposing the model to adversarial examples during training can enhance its
1098 robustness against such attacks He et al. (2023a). Continuous monitoring and updating of the VLMs
1099 are also essential to prevent the introduction of new errors, which should include regular audits and updates
1100 based on the latest medical research and clinical guidelines.

6 CONCLUSION

1101 This review paper highlights the transformative potential of VLMs in generating medical reports and
1102 answering clinical questions from medical images. It explores 16 recent medical VLMs, among which
1103 15 are publicly available. **We observed that 6 of them share a similar architecture that has only recently**
1104 **become common**. These VLMs incorporate a vision encoder, often with a projection module, to produce
1105 visual features, which can be used as input to LLMs. The visual features are then combined with tokenized
1106 text input and fed into the LLM. This approach simplifies model design and leverages the extensive prior
1107 knowledge embedded in LLMs. Furthermore, feeding all data features into LLMs enables the generation

1108 of human-like text outputs, improving user experience and facilitating more effective communication of
1109 medical insights. The review also explores 18 publicly available medical vision-language datasets and
1110 over 10 evaluation metrics for RG and VQA. By providing essential background information, this review
1111 ensures accessibility for readers from the medical field while promoting collaboration between the AI/ML
1112 community and medical professionals.

1113 Moreover, the review highlights the current challenges and potential future directions for VLMs in
1114 medicine. The limited availability of diverse medical datasets and privacy concerns can be addressed through
1115 rigorous data pre-processing and techniques like RAG and FL. Also, since traditional evaluation metrics
1116 often fall short of capturing the nuances of clinical language, there is a need to develop specialized metrics
1117 tailored to medical RG and VQA. It is likewise crucial to address VLM hallucinations, and incorporating
1118 RLHF and RAG are promising solutions. Continual learning methods can help mitigate catastrophic
1119 forgetting, ensuring that models retain the knowledge they have previously acquired. Furthermore,
1120 collaboration between healthcare professionals and AI researchers is essential to deploy VLMs in ways that
1121 genuinely improve patient care. Lastly, ensuring the security of these models is vital, which can be achieved
1122 through robust firewalls and adversarial training. Ultimately, the review serves as a valuable resource for
1123 researchers developing and refining VLMs for medical applications, guiding them in overcoming key
1124 obstacles and leveraging innovative approaches to enhance model performance and clinical integration.

CONFLICT OF INTEREST STATEMENT

1125 The authors declare that the research was conducted in the absence of any commercial or financial
1126 relationships that could be construed as a potential conflict of interest.

AUTHOR CONTRIBUTIONS

1127 IH wrote the first draft of the paper. IH, GR edited and reviewed the paper. GR provided funding.

FUNDING

1128 This work was partly supported by NSF awards 1903466, 2234836, and 2234468.

REFERENCES

1129 Abacha, A. B., Datla, V. V., Hasan, S. A., Demner-Fushman, D., and Müller, H. (2020). Overview of the
1130 vqa-med task at imageclef 2020: Visual question answering and generation in the medical domain. In
1131 *CLEF 2020 Working Notes*. CEUR Workshop Proceedings

1132 Abacha, A. B., Hasan, S. A., Datla, V., Liu, J., Demner-Fushman, D., and Müller, H. (2019). Vqa-med:
1133 Overview of the medical visual question answering task at imageclef 2019. In *Conference and Labs of
1134 the Evaluation Forum*

1135 Acosta, J. N., Falcone, G. J., Rajpurkar, P., and Topol, E. J. (2022). Multimodal biomedical ai. *Nature
1136 Medicine* 28, 1773–1784. doi:10.1038/s41591-022-01981-2

1137 Ahmed, S., Nielsen, I. E., Tripathi, A., Siddiqui, S., Ramachandran, R. P., and Rasool, G. (2023).
1138 Transformers in time-series analysis: A tutorial. *Circuits, Systems, and Signal Processing* 42, 7433–7466

1139 Alayrac, J.-B., Donahue, J., Luc, P., Miech, A., Barr, I., Hasson, Y., et al. (2022). Flamingo: A visual
1140 language model for few-shot learning. In *Advances in Neural Information Processing Systems*. vol. 35,
1141 23716–23736

1142 Allan, M., Kondo, S., Bodenstedt, S., Leger, S., Kadkhodamohammadi, R., Luengo, I., et al. (2020). 2018
1143 robotic scene segmentation challenge. *arXiv Preprint arXiv:2001.11190*

1144 Allan, M., Shvets, A., Kurmann, T., Zhang, Z., Duggal, R., Su, Y.-H., et al. (2019). 2017 robotic instrument
1145 segmentation challenge. *arXiv Preprint arXiv:1902.06426*

1146 Antol, S., Agrawal, A., Lu, J., Mitchell, M., Batra, D., Zitnick, C. L., et al. (2015). VQA: Visual
1147 question answering. In *IEEE International Conference on Computer Vision (ICCV)*. 2425–2433.
1148 doi:10.1109/ICCV.2015.279

1149 Bai, J., Bai, S., Yang, S., Wang, S., Tan, S., Wang, P., et al. (2023a). Qwen-vl: A versatile vision-language
1150 model for understanding, localization, text reading, and beyond. *arXiv Preprint arXiv:2308.12966*

1151 Bai, L., Islam, M., and Ren, H. (2023b). Cat-vil: Co-attention gated vision-language embedding for visual
1152 question localized-answering in robotic surgery. In *Medical Image Computing and Computer Assisted
1153 Intervention – MICCAI*. 397–407. doi:10.1007/978-3-031-43996-4_38

1154 Bai, S. and An, S. (2018). A survey on automatic image caption generation. *Neurocomputing* 311.
1155 doi:10.1016/j.neucom.2018.05.080

1156 Bajwa, J., Munir, U., Nori, A., and Williams, B. (2021). Artificial intelligence in healthcare: Transforming
1157 the practice of medicine. *Future Healthcare Journal* 8, e188–e194. doi:10.7861/fhj.2021-0095

1158 Baldi, P. (2021). *Deep Learning in Science* (Cambridge University Press). doi:10.1017/9781108955652

1159 Banerjee, S. and Lavie, A. (2005). METEOR: An automatic metric for MT evaluation with improved
1160 correlation with human judgments. In *ACL Workshop on Intrinsic and Extrinsic Evaluation Measures
1161 for Machine Translation and/or Summarization*. 65–72

1162 Bannur, S., Hyland, S., Liu, Q., Pérez-García, F., Ilse, M., Castro, D. C., et al. (2023). Learning to exploit
1163 temporal structure for biomedical vision-language processing. *arXiv Preprint arXiv:2301.04558*

1164 Barhoumi, Y., Bouaynaya, N. C., and Rasool, G. (2023). Efficient Scopeformer: Toward Scalable and Rich
1165 Feature Extraction for Intracranial Hemorrhage Detection. *IEEE Access* 11, 81656–81671

1166 Bazi, Y., Rahhal, M. M. A., Bashmal, L., and Zuair, M. (2023). Vision–language model for visual question
1167 answering in medical imagery. *Bioengineering* 10, 380. doi:10.3390/bioengineering10030380

1168 Beam, A., Kompa, B., Schmaltz, A., Fried, I., Weber, G. M., Palmer, N. P., et al. (2020). Clinical
1169 concept embeddings learned from massive sources of multimodal medical data. *Pacific Symposium on
1170 Biocomputing* 25, 295–306. doi:10.1142/9789811215636_0027

1171 Ben Abacha, A., Shivade, C., and Demner-Fushman, D. (2019). Overview of the MEDIQA 2019 shared
1172 task on textual inference, question entailment and question answering. In *BioNLP Workshop and Shared
1173 Task*. 370–379

1174 Bigolin Lanfredi, R., Zhang, M., Auffermann, W. F., Chan, J., Duong, P.-A. T., Srikumar, V., et al. (2022).
1175 Reflacr, a dataset of reports and eye-tracking data for localization of abnormalities in chest x-rays.
1176 *Scientific Data* 9. doi:10.1038/s41597-022-01441-z

1177 Boecking, B., Usuyama, N., Bannur, S., Castro, D. C., Schwaighofer, A., Hyland, S., et al. (2022). Making
1178 the most of text semantics to improve biomedical vision–language processing. In *Computer Vision –
1179 ECCV*. 1–21. doi:10.1007/978-3-031-20059-5_1

1180 Bojanowski, P., Grave, E., Joulin, A., and Mikolov, T. (2017). Enriching word vectors with subword
1181 information. *Transactions of the Association for Computational Linguistics* 5, 135–146. doi:10.1162/
1182 tacl_a_00051

1183 Bommasani, R., Hudson, D. A., Adeli, E., Altman, R., Arora, S., von Arx, S., et al. (2022). On the
1184 Opportunities and Risks of Foundation Models. *arXiv Preprint arXiv:2108.07258*

1185 Brown, T. B., Mann, B., Ryder, N., Subbiah, M., Kaplan, J., Dhariwal, P., et al. (2020). Language models
1186 are few-shot learners. In *Advances in Neural Information Processing Systems*. vol. 33, 1877–1901

1187 Cai, Y. and Rostami, M. (2024). Dynamic transformer architecture for continual learning of multimodal
1188 tasks. *arXiv Preprint arXiv:2401.15275*

1189 Carion, N., Massa, F., Synnaeve, G., Usunier, N., Kirillov, A., and Zagoruyko, S. (2020). End-to-end
1190 object detection with transformers. In *European conference on computer vision*. 213–229. doi:10.1007/
1191 978-3-030-58452-8_13

1192 Chen, F., Zhang, D., Han, M., Chen, X., Shi, J., Xu, S., et al. (2023). VLP: A survey on vision-language
1193 pre-training. *Machine Intelligence Research* 20, 38–56. doi:10.1007/s11633-022-1369-5

1194 Chen, R. J., Ding, T., Lu, M. Y., Williamson, D. F. K., Jaume, G., Song, A. H., et al. (2024). Towards
1195 a general-purpose foundation model for computational pathology. *Nature medicine* 30, 850–862.
1196 doi:10.1038/s41591-024-02857-3

1197 Chen, T., Kornblith, S., Norouzi, M., and Hinton, G. (2020a). A simple framework for contrastive learning
1198 of visual representations. *arXiv Preprint arXiv:2002.05709*

1199 Chen, Y.-C., Li, L., Yu, L., Kholy, A. E., Ahmed, F., Gan, Z., et al. (2020b). UNITER: Universal
1200 image-tExt representation learning. In *European Conference on Computer Vision*. 104–120. doi:10.
1201 1007/978-3-030-58577-8_7

1202 Cherti, M., Beaumont, R., Wightman, R., Wortsman, M., Ilharco, G., Gordon, C., et al. (2022).
1203 Reproducible scaling laws for contrastive language-image learning. *arXiv Preprint arXiv:2212.07143*

1204 Chiang, W.-L., Li, Z., Lin, Z., Sheng, Y., Wu, Z., Zhang, H., et al. (2023). Vicuna: An open-source chatbot
1205 impressing gpt-4 with 90%* chatgpt quality. [Website: <https://lmsys.org/blog/2023-03-30-vicuna/>.
1206 Accessed 20-Feb-2024]

1207 Cho, J., Lei, J., Tan, H., and Bansal, M. (2021). Unifying vision-and-language tasks via text generation. In
1208 *International Conference on Machine Learning*. vol. 139, 1931–1942

1209 Cho, K., van Merriënboer, B., Çaglar Gülcöhre, Bahdanau, D., Bougares, F., Schwenk, H., et al. (2014).
1210 Learning phrase representations using rnn encoder–decoder for statistical machine translation. In
1211 *Conference on Empirical Methods in Natural Language Processing*. 1724–1734. doi:10.3115/v1/
1212 D14-1179

1213 Chowdhery, A., Narang, S., Devlin, J., Bosma, M., Mishra, G., Roberts, A., et al. (2022). Palm: Scaling
1214 language modeling with pathways. *Journal of Machine Learning Research* 24, 1–113

1215 Clunie, D., Taylor, A., Bisson, T., Gutman, D., Xiao, Y., Schwarz, C. G., et al. (2024). Summary of the
1216 national cancer institute 2023 virtual workshop on medical image de-identification—part 2: Pathology
1217 whole slide image de-identification, de-facing, the role of ai in image de-identification, and the nci midi
1218 datasets and pipeline. *Journal of Imaging Informatics in Medicine* doi:10.1007/s10278-024-01183-x

1219 Coronato, A., Naeem, M., De Pietro, G., and Paragliola, G. (2020). Reinforcement learning for intelligent
1220 healthcare applications: A survey. *Artificial Intelligence in Medicine* 109, 101964. doi:10.1016/j.artmed.
1221 2020.101964

1222 Dai, W., Li, J., Li, D., Tiong, A. M. H., Zhao, J., Wang, W., et al. (2023). Instructblip: Towards
1223 general-purpose vision-language models with instruction tuning. *arXiv Preprint arXiv:2305.06500*

1224 Demner-Fushman, D., Kohli, M. D., Rosenman, M. B., Shooshan, S. E., Rodriguez, L. M., Antani, S. K.,
1225 et al. (2015). Preparing a collection of radiology examinations for distribution and retrieval. *Journal of*
1226 *the American Medical Informatics Association (JAMIA)* 23, 304–310. doi:10.1093/jamia/ocv080

1227 Deng, J., Dong, W., Socher, R., Li, L.-J., Li, K., and Fei-Fei, L. (2009). Imagenet: A large-scale hierarchical
1228 image database. In *2009 IEEE Conference on Computer Vision and Pattern Recognition*. 248–255.
1229 doi:10.1109/CVPR.2009.5206848

1230 Devlin, J., Chang, M.-W., Lee, K., and Toutanova, K. (2019). BERT: Pre-training of deep bidirectional
1231 transformers for language understanding. In *Conference of the North American Chapter of the*
1232 *Association for Computational Linguistics*. vol. 1, 4171–4186. doi:10.18653/v1/N19-1423

1233 Dosovitskiy, A., Beyer, L., Kolesnikov, A., Weissenborn, D., Zhai, X., Unterthiner, T., et al. (2021). An
1234 image is worth 16x16 words: Transformers for image recognition at scale. In *International Conference*
1235 *on Learning Representations*

1236 Dou, Z.-Y., Xu, Y., Gan, Z., Wang, J., Wang, S., Wang, L., et al. (2022). An empirical study of training
1237 end-to-end vision-and-language transformers. In *IEEE/CVF Conference on Computer Vision and Pattern*
1238 *Recognition (CVPR)*. 18145–18155. doi:10.1109/CVPR52688.2022.01763

1239 Dwork, C. (2006). Differential privacy. In *Automata, Languages and Programming* (Springer Berlin
1240 Heidelberg), 1–12. doi:10.1007/11787006_1

1241 Eslami, S., Meinel, C., and De Melo, G. (2023). Pubmedclip: How much does clip benefit visual question
1242 answering in the medical domain? In *Findings of the Association for Computational Linguistics*.
1243 1181–1193. doi:10.18653/v1/2023.findings-eacl.88

1244 Esser, P., Rombach, R., and Ommer, B. (2021). Taming transformers for high-resolution image synthesis.
1245 In *2021 IEEE/CVF Conference on Computer Vision and Pattern Recognition (CVPR)*. 12868–12878.
1246 doi:10.1109/CVPR46437.2021.01268

1247 Gan, Z., Li, L., Li, C., Wang, L., Liu, Z., and Gao, J. (2022). Vision-language pre-training: Basics, recent
1248 advances, and future trends. *arXiv Preprint arXiv:2210.09263*

1249 Goodfellow, I., Bengio, Y., and Courville, A. (2016). *Deep Learning* (The MIT Press). <http://www.deeplearningbook.org>

1250 Gu, J., Han, Z., Chen, S., Beirami, A., He, B., Zhang, G., et al. (2023). A systematic survey of prompt
1251 engineering on vision-language foundation models. *arXiv Preprint arXiv:2307.12980*

1252 Gu, Y., Tinn, R., Cheng, H., Lucas, M., Usuyama, N., Liu, X., et al. (2021). Domain-specific language
1253 model pretraining for biomedical natural language processing. *ACM Transactions on Computing for*
1254 *Healthcare* 3, 23. doi:10.1145/3458754

1255 Han, T., Adams, L. C., Papaioannou, J.-M., Grundmann, P., Oberhauser, T., Löser, A., et al. (2023).
1256 Medalpaca – an open-source collection of medical conversational ai models and training data. *arXiv*
1257 *Preprint arXiv:2304.08247*

1258 Hao, Y., Mendelsohn, S., Sterneck, R., Martinez, R., and Frank, R. (2020). Probabilistic predictions of
1259 people perusing: Evaluating metrics of language model performance for psycholinguistic modeling.
1260 *arXiv Preprint arXiv:2009.03954*

1261 He, B., Jia, X., Liang, S., Lou, T., Liu, Y., and Cao, X. (2023a). Sa-attack: Improving
1262 adversarial transferability of vision-language pre-training models via self-augmentation. *arXiv Preprint*
1263 *arXiv:2312.04913*

1264 He, K., Mao, R., Lin, Q., Ruan, Y., Lan, X., Feng, M., et al. (2023b). A survey of large language models
1265 for healthcare: from data, technology, and applications to accountability and ethics. *arXiv Preprint*
1266 *arXiv:2310.05694*

1267 He, K., Zhang, X., Ren, S., and Sun, J. (2016). Deep residual learning for image recognition. In *IEEE*
1268 *Conference on Computer Vision and Pattern Recognition*. 770–778. doi:10.1109/CVPR.2016.90

1269 He, X., Zhang, Y., Mou, L., Xing, E., and Xie, P. (2020). Pathvqa: 30000+ questions for medical visual
1270 question answering. *arXiv Preprint arXiv:2003.10286*

1271 Hochreiter, S. and Schmidhuber, J. (1997). Long short-term memory. *Neural Computation* 9, 1735–1780.
1272 doi:10.1162/neco.1997.9.8.1735

1273

1274 Hu, E. J., Shen, Y., Wallis, P., Allen-Zhu, Z., Li, Y., Wang, S., et al. (2022). LoRA: Low-rank adaptation of
1275 large language models. In *International Conference on Learning Representations*

1276 Huang, G., Liu, Z., Pleiss, G., Van Der Maaten, L., and Weinberger, K. (2022). Convolutional networks
1277 with dense connectivity. *IEEE Transactions on Pattern Analysis and Machine Intelligence* 44, 8704–8716.
1278 doi:10.1109/TPAMI.2019.2918284

1279 Huang, Y., Du, C., Xue, Z., Chen, X., Zhao, H., and Huang, L. (2021). What makes multimodal learning
1280 better than single (provably). In *Advances in Neural Information Processing Systems*

1281 Ionescu, B., Müller, H., Péteri, R., Abacha, A. B., Sarrouti, M., Demner-Fushman, D., et al. (2021).
1282 Overview of the imageclef 2021: Multimedia retrieval in medical, nature, internet and social media
1283 applications. In *Experimental IR Meets Multilinguality, Multimodality, and Interaction*. 345–370.
1284 doi:10.1007/978-3-030-85251-1_23

1285 Irvin, J. A., Rajpurkar, P., Ko, M., Yu, Y., Ciurea-Ilcus, S., Chute, C., et al. (2019). CheXpert: A large chest
1286 radiograph dataset with uncertainty labels and expert comparison. In *AAAI Conference on Artificial
1287 Intelligence*. vol. 33, 590–597. doi:10.1609/aaai.v33i01.3301590

1288 Jeong, J., Tian, K., Li, A., Hartung, S., Behzadi, F., Calle, J., et al. (2023). Multimodal image-text matching
1289 improves retrieval-based chest x-ray report generation. *arXiv Preprint arXiv:2303.17579*

1290 Ji, Q. (2020). 5 - computer vision applications. In *Probabilistic Graphical Models for Computer
1291 Vision* (Academic Press), Computer Vision and Pattern Recognition. 191–297. doi:10.1016/
1292 B978-0-12-803467-5.00010-1

1293 Jia, C., Yang, Y., Xia, Y., Chen, Y., Parekh, Z., Pham, H., et al. (2021). Scaling up visual and vision-
1294 language representation learning with noisy text supervision. In *International Conference on Machine
1295 Learning*. vol. 139, 4904–4916

1296 Jiang, A. Q., Sablayrolles, A., Mensch, A., Bamford, C., Chaplot, D. S., de las Casas, D., et al. (2023).
1297 Mistral 7b. *arXiv Preprint arXiv:2310.06825*

1298 Jin, D., Pan, E., Oufattolle, N., Weng, W.-H., Fang, H., and Szolovits, P. (2021). What disease does
1299 this patient have? a large-scale open domain question answering dataset from medical exams. *Applied
1300 Sciences* 11, 6421. doi:10.3390/app11146421

1301 Jin, Q., Dhingra, B., Liu, Z., Cohen, W. W., and Lu, X. (2019). Pubmedqa: A dataset for biomedical
1302 research question answering. In *Conference on Empirical Methods in Natural Language Processing*.
1303 2567–2577. doi:10.18653/v1/D19-1259

1304 Johnson, A. E., Pollard, T. J., Berkowitz, S. J., Greenbaum, N. R., Lungren, M. P., Deng, C.-y., et al.
1305 (2019a). Mimic-cxr, a de-identified publicly available database of chest radiographs with free-text
1306 reports. *Scientific Data* 6. doi:10.1038/s41597-019-0322-0

1307 Johnson, A. E. W., Pollard, T. J., Greenbaum, N. R., Lungren, M. P., Ying Deng, C., Peng, Y., et al.
1308 (2019b). Mimic-cxr-jpg, a large publicly available database of labeled chest radiographs. *arXiv Preprint
1309 arXiv:1901.07042*

1310 Kayser, M., Emde, C., Camburu, O., Parsons, G., Papiez, B., and Lukasiewicz, T. (2022). Explaining chest
1311 x-ray pathologies in natural language. In *International Conference on Medical Image Computing and
1312 Computer-Assisted Intervention (MICCAI)*. vol. 13435, 701–713. doi:10.1007/978-3-031-16443-9_67

1313 Khan, H., Bouaynaya, N. C., and Rasool, G. (2023). The importance of robust features in mitigating
1314 catastrophic forgetting. In *2023 IEEE Symposium on Computers and Communications (ISCC)* (IEEE),
1315 752–757

1316 Khan, H., Bouaynaya, N. C., and Rasool, G. (2024). Brain-inspired continual learning: Robust feature
1317 distillation and re-consolidation for class incremental learning. *IEEE Access*

1318 Kim, J.-H., Jun, J., and Zhang, B.-T. (2018). Bilinear Attention Networks. In *Advances in Neural*
1319 *Information Processing Systems 31*. vol. 31, 1564–1574

1320 Kingma, D. P. and Ba, J. (2014). Adam: A method for stochastic optimization. *International Conference*
1321 *on Learning Representations*

1322 [Dataset] Koutsoubis, N., Waqas, A., Yilmaz, Y., Ramachandran, R. P., Schabath, M., and Rasool, G.
1323 (2024a). Future-Proofing Medical Imaging with Privacy-Preserving Federated Learning and Uncertainty
1324 Quantification: A Review

1325 [Dataset] Koutsoubis, N., Yilmaz, Y., Ramachandran, R. P., Schabath, M., and Rasool, G. (2024b). Privacy
1326 Preserving Federated Learning in Medical Imaging with Uncertainty Estimation

1327 Kwon, G., Cai, Z., Ravichandran, A., Bas, E., Bhotika, R., and Soatto, S. (2023). Masked vision and
1328 language modeling for multi-modal representation learning. *arXiv Preprint arXiv:2208.02131*

1329 Lambert, N., Castricato, L., von Werra, L., and Havrilla, A. (2022). Illustrating reinforcement learning
1330 from human feedback (rlhf). [Website: <https://huggingface.co/blog/rlhf>. Accessed 20-Feb-2024]

1331 Lau, J. J., Gayen, S., Ben Abacha, A., and Demner-Fushman, D. (2018). A dataset of clinically generated
1332 visual questions and answers about radiology images. *Scientific data* 5, 180251. doi:10.1038/sdata.2018.
1333 251

1334 LeCun, Y., Bengio, Y., and Hinton, G. (2015). Deep learning. *Nature* 521, 436–444. doi:10.1038/
1335 nature14539

1336 Lee, H., Lee, D. Y., Kim, W., Kim, J.-H., Kim, T., Kim, J., et al. (2023). Unixgen: A unified vision-language
1337 model for multi-view chest x-ray generation and report generation. *arXiv Preprint arXiv:2302.12172*

1338 Lester, B., Al-Rfou, R., and Constant, N. (2021). The power of scale for parameter-efficient prompt tuning.
1339 *arXiv Preprint arXiv:2104.08691*

1340 Lewis, P., Perez, E., Piktus, A., Petroni, F., Karpukhin, V., Goyal, N., et al. (2020). Retrieval-augmented
1341 generation for knowledge-intensive nlp tasks. In *Neural Information Processing Systems*. vol. 33,
1342 9459–9474

1343 Li, C., Wong, C., Zhang, S., Usuyama, N., Liu, H., Yang, J., et al. (2023a). Llava-med: Training a large
1344 language-and-vision assistant for biomedicine in one day. *arXiv Preprint arXiv:2306.00890*

1345 Li, J., Selvaraju, R. R., Gotmare, A. D., Joty, S., Xiong, C., and Hoi, S. (2021). Align before fuse: Vision
1346 and language representation learning with momentum distillation. In *Advances in Neural Information*
1347 *Processing Systems*

1348 Li, L. H., Yatskar, M., Yin, D., Hsieh, C.-J., and Chang, K.-W. (2019). VisualBERT: A simple and
1349 performant baseline for vision and language. *arXiv Preprint arXiv:1908.03557*

1350 Li, M., Cai, W., Verspoor, K., Pan, S., Liang, X., and Chang, X. (2022). Cross-modal clinical graph
1351 transformer for ophthalmic report generation. In *IEEE/CVF Conference on Computer Vision and Pattern*
1352 *Recognition (CVPR)*. 20624–20633. doi:10.1109/CVPR52688.2022.02000

1353 Li, P., Liu, G., He, J., Zhao, Z., and Zhong, S. (2023b). Masked vision and language pre-training with
1354 unimodal and multimodal contrastive losses for medical visual question answering. In *Medical Image*
1355 *Computing and Computer Assisted Intervention (MICCAI)*. 374–383. doi:10.1007/978-3-031-43907-0-
1356 36

1357 Li, X. L. and Liang, P. (2021). Prefix-tuning: Optimizing continuous prompts for generation. *arXiv*
1358 *Preprint arXiv:2101.00190*

1359 Li, Y., Li, Z., Zhang, K., Dan, R., Jiang, S., and Zhang, Y. (2023c). Chatdoctor: A medical chat model
1360 fine-tuned on a large language model meta-ai (llama) using medical domain knowledge. *Cureus* 15.
1361 doi:10.7759/cureus.40895

1362 Lin, C.-Y. (2004). ROUGE: A package for automatic evaluation of summaries. In *Text Summarization*
1363 *Branches Out*. 74–81

1364 Lin, W., Zhao, Z., Zhang, X., Wu, C., Zhang, Y., Wang, Y., et al. (2023a). Pmc-clip: Contrastive
1365 language-image pre-training using biomedical documents. *arXiv Preprint arXiv:2303.07240*

1366 Lin, Z., Zhang, D., Tao, Q., Shi, D., Haffari, G., Wu, Q., et al. (2023b). Medical visual question answering:
1367 A survey. *Artificial Intelligence in Medicine* 143, 102611. doi:10.1016/j.artmed.2023.102611

1368 Liu, B., Zhan, L.-M., Xu, L., Ma, L., Yang, Y. F., and Wu, X.-M. (2021a). Slake: A semantically-labeled
1369 knowledge-enhanced dataset for medical visual question answering. *IEEE 18th International Symposium*
1370 *on Biomedical Imaging (ISBI)*, 1650–1654doi:10.1109/ISBI48211.2021.9434010

1371 Liu, B., Zhan, L.-M., Xu, L., and Wu, X.-M. (2023a). Medical visual question answering via conditional
1372 reasoning and contrastive learning. *IEEE Transactions on Medical Imaging* 42, 1532–1545. doi:10.
1373 1109/TMI.2022.3232411

1374 Liu, C., Tian, Y., and Song, Y. (2023b). A systematic review of deep learning-based research on radiology
1375 report generation. *arXiv Preprint arXiv:2311.14199*

1376 Liu, F., Eisenschlos, J. M., Piccinno, F., Krichene, S., Pang, C., Lee, K., et al. (2022). Deplot: One-shot
1377 visual language reasoning by plot-to-table translation. *arXiv Preprint arXiv:2212.10505*

1378 Liu, H., Li, C., Wu, Q., and Lee, Y. J. (2023c). Visual instruction tuning. *arXiv Preprint arXiv:2304.08485*

1379 Liu, H., Xue, W., Chen, Y., Chen, D., Zhao, X., Wang, K., et al. (2024). A survey on hallucination in large
1380 vision-language models. *arXiv Preprint arXiv:2402.00253*

1381 Liu, Z., Lin, Y., Cao, Y., Hu, H., Wei, Y., Zhang, Z., et al. (2021b). Swin transformer: Hierarchical
1382 vision transformer using shifted windows. In *International Conference on Computer Vision (ICCV)*.
1383 9992–10002. doi:10.1109/ICCV48922.2021.00986

1384 Lo, K., Wang, L. L., Neumann, M., Kinney, R., and Weld, D. (2020). S2ORC: The semantic scholar
1385 open research corpus. In *Annual Meeting of the Association for Computational Linguistics*. 4969–4983.
1386 doi:10.18653/v1/2020.acl-main.447

1387 Lu, J., Batra, D., Parikh, D., and Lee, S. (2019). ViLBERT: Pretraining task-agnostic visiolinguistic
1388 representations for vision-and-language tasks. In *Advances in Neural Information Processing Systems*.
1389 13–23

1390 Lu, M. Y., Chen, B., Williamson, D. F. K., Chen, R. J., Liang, I., Ding, T., et al. (2024a). A visual-
1391 language foundation model for computational pathology. *Nature medicine* 30, 863–874. doi:10.1038/
1392 s41591-024-02856-4

1393 Lu, M. Y., Chen, B., Williamson, D. F. K., Chen, R. J., Zhao, M., Chow, A. K., et al. (2024b). A multimodal
1394 generative ai copilot for human pathology. *Nature* doi:10.1038/s41586-024-07618-3

1395 Mabotuwana, T., Hall, C. S., and Cross, N. (2020). Framework for extracting critical findings in radiology
1396 reports. *Journal of Digital Imaging* 33, 988–995. doi:10.1007/s10278-020-00349-7

1397 Manzari, O. N., Ahmadabadi, H., Kashiani, H., Shokouhi, S. B., and Ayatollahi, A. (2023). MedViT:
1398 A robust vision transformer for generalized medical image classification. *Computers in Biology and*
1399 *Medicine* 157, 106791. doi:10.1016/j.combiomed.2023.106791

1400 Masci, J., Meier, U., Ciresan, D. C., and Schmidhuber, J. (2011). Stacked convolutional auto-encoders for
1401 hierarchical feature extraction. In *International Conference on Artificial Neural Networks*. vol. 6791,
1402 52–59

1403 Mikolov, T., Chen, K., Corrado, G., and Dean, J. (2013a). Efficient estimation of word representations in
1404 vector space. *arXiv Preprint arXiv:1301.3781*

1405 Mikolov, T., Sutskever, I., Chen, K., Corrado, G. S., and Dean, J. (2013b). Distributed representations of
1406 words and phrases and their compositionality. In *Advances in Neural Information Processing Systems*.
1407 vol. 26, 3111–3119

1408 Mishra, P., Verk, R., Fornasier, D., Piciarelli, C., and Foresti, G. L. (2021). VT-ADL: A vision transformer
1409 network for image anomaly detection and localization. In *IEEE International Symposium on Industrial
1410 Electronics (ISIE)*. 01–06. doi:10.1109/ISIE45552.2021.9576231

1411 Miura, Y., Zhang, Y., Tsai, E., Langlotz, C., and Jurafsky, D. (2021). Improving factual completeness and
1412 consistency of image-to-text radiology report generation. In *North American Chapter of the Association
1413 for Computational Linguistics*. 5288–5304. doi:10.18653/v1/2021.nacl-main.416

1414 Mohsan, M. M., Akram, M. U., Rasool, G., Alghamdi, N. S., Baqai, M. A. A., and Abbas, M. (2023).
1415 Vision transformer and language model based radiology report generation. *IEEE Access* 11, 1814–1824.
1416 doi:10.1109/ACCESS.2022.3232719

1417 Monshi, M. M. A., Poon, J., and Chung, V. (2020). Deep learning in generating radiology reports: A
1418 survey. *Artificial Intelligence in Medicine* 106, 101878. doi:10.1016/j.artmed.2020.101878

1419 Moon, J. H., Lee, H., Shin, W., Kim, Y.-H., and Choi, E. (2022). Multi-modal understanding and generation
1420 for medical images and text via vision-language pre-training. *IEEE Journal of Biomedical and Health
1421 Informatics* 26, 6070–6080. doi:10.1109/JBHI.2022.3207502

1422 Moor, M., Huang, Q., Wu, S., Yasunaga, M., Zakka, C., Dalmia, Y., et al. (2023). Med-Flamingo: A
1423 multimodal medical few-shot learner. *arXiv Preprint arXiv:2307.15189*

1424 Nadkarni, P. M., Ohno-Machado, L., and Chapman, W. W. (2011). Natural language processing: An
1425 Introduction. *Journal of the American Medical Informatics Association* 18, 544–551

1426 Norgeot, B., Muenzen, K., Peterson, T. A., Fan, X., Glicksberg, B. S., Schenk, G., et al. (2020). Protected
1427 health information filter (philter): accurately and securely de-identifying free-text clinical notes. *npj
1428 Digital Medicine* 3. doi:10.1038/s41746-020-0258-y

1429 Ouyang, L., Wu, J., Jiang, X., Almeida, D., Wainwright, C., Mishkin, P., et al. (2022). Training language
1430 models to follow instructions with human feedback. *Advances in neural information processing systems*
1431 35, 27730–27744

1432 Papineni, K., Roukos, S., Ward, T., and Zhu, W.-J. (2002). Bleu: a method for automatic evaluation of
1433 machine translation. In *Annual Meeting of the Association for Computational Linguistics*. 311–318.
1434 doi:10.3115/1073083.1073135

1435 Pelka, O., Koitka, S., Rückert, J., Nensa, F., and Friedrich, C. M. (2018). Radiology objects in context
1436 (roco): A multimodal image dataset. In *Intravascular Imaging and Computer Assisted Stenting and Large-
1437 Scale Annotation of Biomedical Data and Expert Label Synthesis* (Springer International Publishing),
1438 vol. 11043, 180–189. doi:10.1007/978-3-030-01364-6_20

1439 Pellegrini, C., Özsoy, E., Busam, B., Navab, N., and Keicher, M. (2023). Radialog: A large vision-language
1440 model for radiology report generation and conversational assistance. *arXiv Preprint arXiv:2311.18681*

1441 Peng, Y., Wang, X., Lu, L., Bagheri, M., Summers, R. M., and Lu, Z. (2017). Negbio: A high-performance
1442 tool for negation and uncertainty detection in radiology reports. *AMIA Summits on Translational Science
1443 Proceedings* 2018, 188–196

1444 Pennington, J., Socher, R., and Manning, C. (2014). Glove: Global vectors for word representation. In
1445 *Empirical Methods in Natural Language Processing*. vol. 14, 1532–1543. doi:10.3115/v1/D14-1162

1446 Radford, A., Kim, J. W., Hallacy, C., Ramesh, A., Goh, G., Agarwal, S., et al. (2021). Learning transferable
1447 visual models from natural language supervision. *arXiv Preprint arXiv:2103.00020*

1448 Rai, A. and Borah, S. (2021). Study of various methods for tokenization. In *Applications of Internet of
1449 Things*. 193–200. doi:10.1007/978-981-15-6198-6_18

1450 Ramesh, V., Chi, N., and Rajpurkar, P. (2022). Improving radiology report generation systems by removing
1451 hallucinated references to non-existent priors. In *Machine Learning Research*. vol. 193, 456–473

1452 Ranftl, R., Bochkovskiy, A., and Koltun, V. (2021). Vision transformers for dense prediction. In *IEEE/CVF
1453 International Conference on Computer Vision (ICCV)*. 12159–12168. doi:10.1109/ICCV48922.2021.
1454 01196

1455 Rani, V., Nabi, S., Kumar, M., Mittal, A., and Saluja, K. (2023). Self-supervised learning: A succinct
1456 review. *Archives of Computational Methods in Engineering* 30. doi:10.1007/s11831-023-09884-2

1457 Ranjit, M., Ganapathy, G., Manuel, R., and Ganu, T. (2023). Retrieval augmented chest x-ray report
1458 generation using openai gpt models. *arXiv Preprint arXiv:2305.03660*

1459 Reddy, S. (2024). Generative ai in healthcare: an implementation science informed translational path on
1460 application, integration and governance. *Implementation Science* 19. doi:10.1186/s13012-024-01357-9

1461 Ren, M., Cao, B., Lin, H., Liu, C., Han, X., Zeng, K., et al. (2024). Learning or Self-aligning? Rethinking
1462 Instruction Fine-tuning. *arXiv Preprint arXiv:2402.18243*

1463 Rezatofighi, S. H., Tsoi, N., Gwak, J., Sadeghian, A., Reid, I. D., and Savarese, S. (2019). Generalized
1464 intersection over union: A metric and a loss for bounding box regression. *IEEE/CVF Conference on
1465 Computer Vision and Pattern Recognition (CVPR)* , 658–666doi:10.1109/cvpr.2019.00075

1466 Robbins, H. E. (1951). A stochastic approximation method. *Annals of Mathematical Statistics* 22, 400–407.
1467 doi:10.1214/aoms/1177729586

1468 Romanov, A. and Shivade, C. (2018). Lessons from natural language inference in the clinical domain.
1469 In *Conference on Empirical Methods in Natural Language Processing*. 1586–1596. doi:10.18653/v1/
1470 D18-1187

1471 Rückert, J., Ben Abacha, A., García Seco de Herrera, A., Bloch, L., Brügel, R., Idrissi-Yaghir, A., et al.
1472 (2022). Overview of imageclefmedical 2022 – caption prediction and concept detection. In *CEUR
1473 Workshop Proceedings*. vol. 3180, 1294–1307

1474 Schmidt, R. M. (2019). Recurrent neural networks (rnns): A gentle introduction and overview. *arXiv
1475 Preprint arXiv:1912.05911*

1476 Seenivasan, L., Islam, M., Krishna, A. K., and Ren, H. (2022). Surgical-vqa: Visual question answering in
1477 surgical scenes using transformer. In *Medical Image Computing and Computer Assisted Intervention –
1478 MICCAI*. 33–43. doi:10.1007/978-3-031-16449-1_4

1479 Sengupta, S. and Brown, D. E. (2023). Automatic report generation for histopathology images using
1480 pre-trained vision transformers and bert. *arXiv Preprint arXiv:2312.01435*

1481 Sennrich, R., Haddow, B., and Birch, A. (2016). Neural machine translation of rare words with subword
1482 units. In *54th Annual Meeting of the Association for Computational Linguistics (Volume 1: Long Papers)*.
1483 1715–1725. doi:10.18653/v1/P16-1162

1484 Sharma, D., Dhiman, C., and Kumar, D. (2023). Evolution of visual data captioning methods, datasets,
1485 and evaluation metrics: a comprehensive survey. *Expert Systems with Applications* 221, 119773.
1486 doi:10.1016/j.eswa.2023.119773

1487 Shrestha, P., Amgain, S., Khanal, B., Linte, C. A., and Bhattacharai, B. (2023). Medical vision language
1488 pretraining: A survey. *arXiv Preprint arXiv:2312.06224*

1489 Shu, C., Chen, B., Liu, F., Fu, Z., Shareghi, E., and Collier, N. (2023). Visual med-alpaca: A parameter-
1490 efficient biomedical llm with visual capabilities. [Website: [https://cambridgel1.github.io/visual-med-
alpaca/](https://cambridgel1.github.io/visual-med-
1491 alpaca/). Accessed 20-Feb-2024]

1492 Singhal, K., Azizi, S., Tu, T., Mahdavi, S. S., Wei, J., Chung, H. W., et al. (2023). Large language models
1493 encode clinical knowledge. *Nature* 620, 172–180. doi:10.1038/s41586-023-06291-2

1494 Smit, A., Jain, S., Rajpurkar, P., Pareek, A., Ng, A. Y., and Lungren, M. P. (2020). Chexbert: Combining
1495 automatic labelers and expert annotations for accurate radiology report labeling using bert. *arXiv*
1496 *Preprint arXiv:2004.09167*

1497 Soviany, P., Ionescu, R. T., Rota, P., and Sebe, N. (2021). Curriculum learning: A survey. *International*
1498 *Journal of Computer Vision* 130, 1526–1565. doi:10.1007/s11263-022-01611-x

1499 Stripelis, D., Saleem, H., Ghai, T., Dhinagar, N. J., Gupta, U., Anastasiou, C., et al. (2021). Secure
1500 neuroimaging analysis using federated learning with homomorphic encryption. In *SPIE Medical Imaging*.
1501 doi:10.1117/12.2606256

1502 Subramanian, S., Wang, L. L., Mehta, S., Beglin, B., van Zuylen, M., Parasa, S., et al. (2020). Medicat:
1503 A dataset of medical images, captions, and textual references. In *Findings of the Association for*
1504 *Computational Linguistics: EMNLP*. 2112–2120. doi:10.18653/v1/2020.findings-emnlp.191

1505 Sun, Z., Shen, S., Cao, S., Liu, H., Li, C., Shen, Y., et al. (2023). Aligning large multimodal models with
1506 factually augmented rlhf. *arXiv Preprint arXiv:2309.14525*

1507 Sutton, R. and Barto, A. (1998). Reinforcement learning: An introduction. *IEEE Transactions on Neural*
1508 *Networks* 9, 1054–1054. doi:10.1109/TNN.1998.712192

1509 Tan, M. and Le, Q. V. (2020). Efficientnet: Rethinking model scaling for convolutional neural networks.
1510 *arXiv Preprint arXiv:1905.11946*

1511 Tanwani, A. K., Barral, J., and Freedman, D. (2022). Repsnet: Combining vision with language for
1512 automated medical reports. In *Medical Image Computing and Computer Assisted Intervention (MICCAI)*.
1513 714–724. doi:10.1007/978-3-031-16443-9_68

1514 Taylor, W. L. (1953). “cloze procedure”: A new tool for measuring readability. *Journalism & Mass*
1515 *Communication Quarterly* 30, 415–433. doi:10.1177/107769905303000401

1516 Thawkar, O., Shaker, A., Mullappilly, S. S., Cholakkal, H., Anwer, R. M., Khan, S., et al. (2023).
1517 Xraygpt: Chest radiographs summarization using medical vision-language models. *arXiv Preprint*
1518 *arXiv:2306.07971*

1519 Ting, P., Li, P., and Zhao, L. (2023). A survey on automatic generation of medical imaging reports based
1520 on deep learning. *BioMedical Engineering OnLine* 22. doi:10.1186/s12938-023-01113-y

1521 Touvron, H., Lavril, T., Izacard, G., Martinet, X., Lachaux, M.-A., Lacroix, T., et al. (2023a). LLaMA:
1522 Open and efficient foundation language models. *arXiv Preprint arXiv:2302.13971*

1523 Touvron, H., Martin, L., Stone, K., Albert, P., Almahairi, A., Babaei, Y., et al. (2023b). Llama 2: Open
1524 foundation and fine-tuned chat models. *arXiv Preprint arXiv:2307.09288*

1525 Tripathi, A., Waqas, A., Venkatesan, K., Yilmaz, Y., and Rasool, G. (2024a). Building flexible, scalable,
1526 and machine learning-ready multimodal oncology datasets. *Sensors* 24

1527 [Dataset] Tripathi, A., Waqas, A., Yilmaz, Y., and Rasool, G. (2024b). HoneyBee: A Scalable Modular
1528 Framework for Creating Multimodal Oncology Datasets with Foundational Embedding Models

1529 Tyagi, K., Pathak, G., Nijhawan, R., and Mittal, A. (2021). Detecting pneumonia using vision transformer
1530 and comparing with other techniques. In *International Conference on Electronics, Communication and*
1531 *Aerospace Technology (ICECA)*. 12–16. doi:10.1109/ICECA52323.2021.9676146

1532 van den Oord, A., Li, Y., and Vinyals, O. (2019). Representation learning with contrastive predictive
1533 coding. *arXiv Preprint arXiv:1807.03748*

1534 Vaswani, A., Shazeer, N., Parmar, N., Uszkoreit, J., Jones, L., Gomez, A. N., et al. (2017). Attention is all
1535 you need. In *Advances in Neural Information Processing Systems*. vol. 30, 5998–6008

1536 Verspoor, K. and Cohen, K. B. (2013). *Encyclopedia of Systems Biology* (Springer New York), chap.
1537 Natural Language Processing. 1495–1498. doi:10.1007/978-1-4419-9863-7_158

1538 Wang, C., Cho, K., and Gu, J. (2020). Neural machine translation with byte-level subwords. In *AAAI Conference on Artificial Intelligence*. 9154–9160. doi:10.1609/aaai.v34i05.6451

1539

1540 Wang, J., Yang, Z., Hu, X., Li, L., Lin, K., Gan, Z., et al. (2022a). Git: A generative image-to-text transformer for vision and language. *arXiv Preprint arXiv:2205.14100*

1541

1542 Wang, L., Zhang, X., Su, H., and Zhu, J. (2023a). A comprehensive survey of continual learning: Theory, method and application. *arXiv Preprint arXiv:2302.00487*

1543

1544 Wang, Y., Kordi, Y., Mishra, S., Liu, A., Smith, N. A., Khashabi, D., et al. (2023b). Self-instruct: Aligning language models with self-generated instructions. *arXiv Preprint arXiv:2212.10560*

1545

1546 Wang, Z., Wu, Z., Agarwal, D., and Sun, J. (2022b). Medclip: Contrastive learning from unpaired medical images and text. *arXiv Preprint arXiv:2210.10163*

1547

1548 Wang, Z., Yu, J., Yu, A. W., Dai, Z., Tsvetkov, Y., and Cao, Y. (2022c). Simvlm: Simple visual language model pretraining with weak supervision. In *International Conference on Learning Representations (ICLR)*

1549

1550

1551 Waqas, A., Bui, M. M., Glassy, E. F., El Naqa, I., Borkowski, P., Borkowski, A. A., et al. (2023). Revolutionizing Digital Pathology With the Power of Generative Artificial Intelligence and Foundation Models. *Laboratory Investigation* 103, 100255. doi:<https://doi.org/10.1016/j.labinv.2023.100255>

1552

1553

1554 Waqas, A., Naveed, J., Shahnawaz, W., Asghar, S., Bui, M. M., and Rasool, G. (2024a). Digital pathology and multimodal learning on oncology data. *BJR—Artificial Intelligence* 1, 1–15

1555

1556 Waqas, A., Tripathi, A., Ramachandran, R. P., Stewart, P. A., and Rasool, G. (2024b). Multimodal Data Integration for Oncology in the Era of Deep Neural Networks: A Review. *Frontiers in Artificial Intelligence* 7. doi:10.3389/frai.2024.1408843

1557

1558

1559 [Dataset] Waqas, A., Tripathi, A., Stewart, P., Naeini, M., and Rasool, G. (2024c). Embedding-based Multimodal Learning on Pan-Squamous Cell Carcinomas for Improved Survival Outcomes

1560

1561 Wu, Y., Schuster, M., Chen, Z., Le, Q. V., Norouzi, M., Macherey, W., et al. (2016). Google’s neural machine translation system: Bridging the gap between human and machine translation. *arXiv Preprint arXiv:1609.08144*

1562

1563

1564 Xie, S., Girshick, R. B., Dollár, P., Tu, Z., and He, K. (2016). Aggregated residual transformations for deep neural networks. *IEEE Conference on Computer Vision and Pattern Recognition (CVPR)*, 5987–5995doi:10.1109/CVPR.2017.634

1565

1566

1567 Xie, Z., Zhang, Z., Cao, Y., Lin, Y., Bao, J., Yao, Z., et al. (2022). Simmim: A simple framework for masked image modeling. *IEEE/CVF Conference on Computer Vision and Pattern Recognition (CVPR)*, 9643–9653

1568

1569

1570 Xin, C., Liu, Z., Zhao, K., Miao, L., Ma, Y., Zhu, X., et al. (2022). An improved transformer network for skin cancer classification. *Computers in Biology and Medicine* 149, 105939. doi:10.1016/j.combiomed.2022.105939

1571

1572

1573 Xu, M., Islam, M., Lim, C. M., and Ren, H. (2021). Learning domain adaptation with model calibration for surgical report generation in robotic surgery. *2021 IEEE International Conference on Robotics and Automation (ICRA)*, 12350–12356doi:10.1109/ICRA48506.2021.9561569.

1574

1575

1576 Yamashita, R., Nishio, M., Do, R., and Togashi, K. (2018). Convolutional neural networks: an overview and application in radiology. *Insights into Imaging* 9. doi:10.1007/s13244-018-0639-9

1577

1578 Yang, X., Chen, A., Pournejatian, N. M., Shin, H.-C., Smith, K. E., Parisien, C., et al. (2022). A large language model for electronic health records. *NPJ Digital Medicine* 5. doi:10.1038/s41746-022-00742-2

1579

1580 Yu, F., Endo, M., Krishnan, R., Pan, I., Tsai, A., Reis, E., et al. (2023). Evaluating progress in automatic chest x-ray radiology report generation. *Patterns* 4, 100802. doi:10.1016/j.patter.2023.100802

1581

1582 Yuan, Z., Jin, Q., Tan, C., Zhao, Z., Yuan, H., Huang, F., et al. (2023). Ramm: Retrieval-augmented
1583 biomedical visual question answering with multi-modal pre-training. *arXiv Preprint arXiv:2303.00534*

1584 Zellers, R., Bisk, Y., Farhadi, A., and Choi, Y. (2019). From recognition to cognition: Visual commonsense
1585 reasoning. In *IEEE/CVF Conference on Computer Vision and Pattern Recognition (CVPR)*. 6713–6724.
1586 doi:10.1109/CVPR.2019.00688

1587 Zeng, G., Yang, W., Ju, Z., Yang, Y., Wang, S., Zhang, R., et al. (2020). MedDialog: Large-scale medical
1588 dialogue datasets. In *Conference on Empirical Methods in Natural Language Processing (EMNLP)*.
1589 9241–9250. doi:10.18653/v1/2020.emnlp-main.743

1590 Zhai, Y., Tong, S., Li, X., Cai, M., Qu, Q., Lee, Y. J., et al. (2023). Investigating the catastrophic forgetting
1591 in multimodal large language models. *arXiv Preprint arXiv:2309.10313*

1592 Zhan, L.-M., Liu, B., Fan, L., Chen, J., and Wu, X.-M. (2020). Medical visual question answering
1593 via conditional reasoning. In *The 28th ACM International Conference on Multimedia*. 2345–2354.
1594 doi:10.1145/3394171.3413761

1595 Zhang, C., Xie, Y., Bai, H., Yu, B., Li, W., and Gao, Y. (2021). A survey on federated learning.
1596 *Knowledge-Based Systems* 216, 106775. doi:10.1016/j.knosys.2021.106775

1597 Zhang, H., Niu, Y., and Chang, S.-F. (2018). Grounding referring expressions in images by variational
1598 context. In *IEEE/CVF Conference on Computer Vision and Pattern Recognition*. 4158–4166. doi:10.
1599 1109/CVPR.2018.00437

1600 Zhang, S., Xu, Y., Usuyama, N., Bagga, J., Tinn, R., Preston, S., et al. (2023a). Large-scale domain-specific
1601 pretraining for biomedical vision-language processing. *arXiv Preprint arXiv:2303.00915*

1602 Zhang, T., Kishore, V., Wu, F., Weinberger, K. Q., and Artzi, Y. (2020). Bertscore: Evaluating text
1603 generation with bert. In *International Conference on Learning Representations*

1604 Zhang, W., Huang, Y., Zhang, T., Zou, Q., Zheng, W.-S., and Wang, R. (2023b). Adapter learning in
1605 pretrained feature extractor for continual learning of diseases. *arXiv Preprint arXiv:2304.09042*

1606 Zhang, Y., Chen, Q., Yang, Z., Lin, H., and Lu, Z. (2019). Biowordvec, improving biomedical word
1607 embeddings with subword information and mesh. *Scientific Data* 6. doi:10.1038/s41597-019-0055-0

1608 Zhao, R., Chen, H., Wang, W., Jiao, F., Do, X. L., Qin, C., et al. (2023). Retrieving multimodal information
1609 for augmented generation: A survey. *arXiv Preprint arXiv:2303.10868*

1610 Zhen, L., Hu, P., Wang, X., and Peng, D. (2019). Deep supervised cross-modal retrieval. In *IEEE/CVF*
1611 *Conference on Computer Vision and Pattern Recognition (CVPR)*. 10386–10395. doi:10.1109/CVPR.
1612 2019.01064

1613 Zhou, D.-W., Zhang, Y., Ning, J., Ye, H.-J., Zhan, D.-C., and Liu, Z. (2023a). Learning without forgetting
1614 for vision-language models. *arXiv Preprint arXiv:2305.19270*

1615 Zhou, H., Gu, B., Zou, X., Li, Y., Chen, S. S., Zhou, P., et al. (2023b). A survey of large language models
1616 in medicine: Progress, application, and challenge. *arXiv Preprint arXiv:2311.05112*

1617 Ziegler, D. M., Stiennon, N., Wu, J., Brown, T. B., Radford, A., Amodei, D., et al. (2020). Fine-tuning
1618 language models from human preferences. *arXiv Preprint arXiv:1909.08593*